International Journal of Nanomedicine

Dovepress
open access to scientific and medical research

Open Access Full Text Article

ORIGINAL RESEARCH

# Comparison of cytocompatibility and anticancer properties of traditional and green chemistry-synthesized tellurium nanowires

This article was published in the following Dove Medical Press journal:
*International Journal of Nanomedicine*



Ada Vernet Crua[1–3,*]
David Medina[1,2,*]
Bohan Zhang[1,2]
María Ujué González[4]
Yves Huttel[5]
José Miguel García-Martín[4]
Jorge L Cholula-Díaz[6]
Thomas J Webster[1,2]

[1]Department of Chemical Engineering, Northeastern University, Boston, MA, USA; [2]Nanomedicine Science and Technology Center, Northeastern University, Boston, MA, USA; [3]Universitat Rovira I Virgili, Tarragona, Spain; [4]Instituto de Micro y Nanotechnologia, IMN-CNM, CSIC (CEI UAM+CSIC), Tres Cantos, Spain; [5]Materials Science Factory, Instituto de Ciencias de Materiales, ICMN-CSIC, Madrid, Spain; [6]School of Engineering and Sciences, Tecnologico de Monterrey, Monterrey, NL, Mexico

*These authors contributed equally to this work

Correspondence: Thomas J Webster
Department of Chemical Engineering, Northeastern University, 313 Snell Engineering Center, 360 Huntington Avenue, Boston, MA 02115, USA
Tel +1 617 373 6585
Fax +1 617 373 2209
Email th.webster@neu.edu

**Background:** Traditional physicochemical approaches for the synthesis of compounds, drugs, and nanostructures developed as potential solutions for antimicrobial resistance or against cancer treatment are, for the most part, facile and straightforward. Nevertheless, these approaches have several limitations, such as the use of toxic chemicals and production of toxic by-products with limited biocompatibility. Therefore, new methods are needed to address these limitations, and green chemistry offers a suitable and novel answer, with the safe and environmentally friendly design, manufacturing, and use of minimally toxic chemicals. Green chemistry approaches are especially useful for the generation of metallic nanoparticles or nanometric structures that can effectively and efficiently address health care concerns.

**Objective:** Here, tellurium (Te) nanowires were synthesized using a novel green chemistry approach, and their structures and cytocompatibility were evaluated.

**Method:** An easy and straightforward hydrothermal method was employed, and the Te nanowires were characterized using transmission electron microscopy, scanning electron microscopy, energy-dispersive X-ray spectroscopy, Fourier-transform infrared spectroscopy, X-ray powder diffraction, X-ray photoelectron spectroscopy, and optical microscopy for morphology, size, and chemistry. Cytotoxicity tests were performed with human dermal fibroblasts and human melanoma cells (to assess anticancer properties). The results showed that a treatment with Te nanowires at concentrations between 5 and 100 µg/mL improved the proliferation of healthy cells and decreased cancerous cell growth over a 5-day period. Most importantly, the green chemistry -synthesized Te nanowires outperformed those produced by traditional synthetic chemical methods.

**Conclusion:** This study suggests that green chemistry approaches for producing Te nanostructures may not only reduce adverse environmental effects resulting from traditional synthetic chemistry methods, but also be more effective in numerous health care applications.

**Keywords:** nanowires, tellurium, biocompatibility, anticancer, green chemistry

## Introduction

In a world of constant duality where the population density increases as dramatically as natural resources disappear, there are some concerns that arise from the increased use of synthetic chemicals in society. Traditional chemistry has undoubtedly enhanced the quality of life, but at a price of threatening the environment and, in some cases, human health. Chemical processes, to a certain extent, are responsible for the contamination of all the known ecosystems all over the world.[1–3]

This is especially true for nanotechnology or nanomaterials. Nanotechnology produces materials at a small scale that have novel properties much different from those of the bulk materials. In recent years, the increased implementation of nanotechnology has provided solutions for specific problems including antimicrobial resistance,[4–6] cancer treatments,[7–9] bioimaging,[10,11] and drug delivery.[12–14] The traditional physicochemical approaches for the synthesis of nanomaterials involve easy and straightforward protocols, using available techniques such as laser ablation[15,16] or chemical vapor deposition.[17,18] Nevertheless, there is a cost associated with these synthesis methods, such as the production of toxic by-products, the use of harsh chemicals, and lack of biocompatibility of the nanomaterials, if not pure.

Another worldwide concern is cancer, which is defined as the uncontrollable growth of cells and the abnormal behavior of cells.[19–21] It is stated to be the second cause of death in the USA, with >1.7 million estimated cases each year.[22,23] There are potential known cancer treatments such as chemotherapy,[24] radiotherapy,[25] and surgery;[26] nevertheless, they present a huge variety of side effects including fatigue, anemia, and death.[27,28] Therefore, there is a need to find alternative treatments that avoid these limitations. Here, nanotechnology – with the synthesis of different nanostructures – can be considered a solution, as cancer cells do not have the mechanism to eliminate some metallic structures, unlike normal cells that have this ability, leading to selective cancer cell death while maintaining the viability of healthy cells.[29,30]

Therefore, new methods are needed, and green chemistry offers a suitable and novel answer, with the safe and environmentally friendly design, manufacturing, and use of chemical products that do not produce toxic and harsh by-products.[31,32]

Green chemistry is considered an alternative approach in that it combines materials coming from synthetic chemistry and nature to overcome issues from traditional synthesis. Green chemistry approaches are especially useful for the generation of metallic nanoparticles (NPs), which have nanometric structures that effectively and efficiently address concerns in both health care and industrial applications.[33–35] Therefore, these approaches offer the chance to use living organisms (such as bacteria,[36] human cells,[37,38] fungi,[39] or plants[40,41]) as well as dietary and organic natural compounds (such as coffee,[42] tea, or honey extracts[43]) or biological waste materials produced from industrial alimentary plants,[44] to naturally synthesize NPs. These nanostructures exhibit antibacterial and/or anticancer properties and can be used as drug delivery carriers and in industrial applications. These approaches are cost-effective and environmentally friendly, using standard reaction parameters in redox-reduction or hydrothermal techniques to generate specifically metallic nanostructures with a high throughput.

Several studies have implemented green nanotechnology for the synthesis of nanostructures to exhibit low cytotoxicity to human cells. For instance, garlic extract has been used to synthesize silver NPs with no cytotoxicity for fibroblasts,[45] and Mukherjee et al used gold NPs synthesized using plant leaves to show both biocompatibility and anticancer properties against breast cancer cells.[46] With such a promise shown in previous studies, there has been an increased interest in the generation of green NPs that also have anticancer properties. For example, copper oxide NPs made by Rehana et al[47] and silver NPs produced by Kelkawi et al[48] that were both synthesized using different plant extracts showed attractive anticancer properties.

There are also plenty of studies that compare the effect of the NP synthesis method (ie, green or traditional synthetic chemistry) on the anticancer, antimicrobial, and biocompatibility properties. These studies have shown continuously that NPs made using green approaches are nontoxic or less toxic than those produced by traditional synthetic processes. For example, nickel NPs made from root extracts were nontoxic to mammalian cells compared with the same ones made using conventional chemistry.[49]

During the past years, as mentioned earlier, different methodologies have been studied to produce NPs. For instance, Liu et al prepared tellurium (Te) nanotubes with a controllable size and morphology by using a microwave approach and monosaccharides as reducing agents.[50] Another approach is via hydrothermal reactions, which use high pressure and temperature in addition to water and the organic compound to obtain metallic NPs.[51,52] Different materials have been reported to work, such as platinum[53] or titanium oxide[54] NPs for the catalytic industry, and Te, a rare metalloid, is also considered a good candidate.[55,56] Te nanowires (TeNWs) have been synthesized by employing hydrothermal reactions mainly for semiconductor and catalytic applications;[57,58] however, their biomedical applications are largely unknown, as Te – even has similarities with oxygen, selenium, or sulfur – is not a trace element, and it has not been considered for biochemical interests. Nevertheless, some compounds of Te including tellurides ($Te^{2-}$) and tellurites ($TeO_3^{2-}$) are known to inhibit different proteins and enzymes and are capable of killing microorganisms such as bacteria and plasmodia. Besides, they can induce apoptosis in certain cancer cells.[59] As Sredni mentioned, two Te compounds – ammonium trichloro(dioxoethylene-O,O')tellurate (AS101) and octa-O-bis-(R,R)-tartarate ditellurane – have been reported as anticancer agents by modulating the enzymatic activity and inhibiting tumor proliferation.[60]

As a consequence, Te has been considered a good candidate for biological applications. There are only a few reports on their antibacterial properties against *Escherichia coli* and *Staphylococcus aureus* showing much promise, using TeNWs nanowires made from the fungus *Aspergillus welwitschiae*[61] and a combination of Te and Au nanowires over a carbon surface using a chemical approach with hydrazine.[62] Low cytotoxicity on mammalian epithelial cells was reported for the latter.

In this research, for the first time, TeNWs were synthesized using both traditional synthetic and green approaches, and their properties were compared. The two ways to synthesize such nanowires were as follows: 1) a clean (green) and cost-effective hydrothermal synthesis employing Te salt and starch and 2) a traditional approach using metallic salt and chemical synthetic reducing agents such as ammonia ($NH_3$) and hydrazine. Both methods were similar in subsequent reaction conditions. After purification, the nanostructures were characterized using transmission electron microscopy (TEM), scanning electron microscopy (SEM), energy-dispersive X-ray (EDX) spectroscopy, Fourier transform infrared spectroscopy (FT-IR), X-ray powder diffraction (XRD), X-ray photoelectron spectroscopy (XPS), and optical microscopy regarding morphology, size, and composition. Cytocompatibility and anticancer properties of the chemically synthesized TeNWs (CHEM-TeNWs) and green-synthesized TeNWs (GREEN-TeNWs) were compared. Cytotoxicity assays were performed over 5 days with both human dermal fibroblast (HDF) cells and human melanoma cancer cells. The results showed much promise for the further study of GREEN-TeNWs compared with CHEM-TeNWs for numerous medical applications.

# Materials and methods

## TeNW synthesis and purification

Following a variation of the protocol described by Hong et al,[55] in a typical process of integration, sodium tellurite ($Na_2TeO_3$; Sigma-Aldrich, St Louis, MO, USA) was mixed with 1 g of polyvinylpyrrolidone (PVP; Sigma-Aldrich) and dissolved in 30 mL of deionized water. Next, 1.5 mL of hydrazine hydrate (Sigma-Aldrich) and 3 mL of an $NH_3$ (Sigma-Aldrich) solution (25% w/w) were added. The solution was stirred at a room temperature, then transferred into a teflon-lined stainless steel reactor and placed into an oven at 180°C for 4 hours. After the reaction, the mixture was allowed to cool down at a room temperature.

For the green synthesis route, the procedure was followed as described by Lu et al.[56] with some modifications. Briefly, telluric acid ($H_2TeO_4$; Sigma-Aldrich) was mixed with 0.15 g of a starch (Sigma-Aldrich) solution in deionized water. Then, the mixture was transferred into a teflon-lined stainless steel reactor and placed into an oven at 160°C for 15 hours. The mixture was then allowed to cool down at a room temperature.

At a room temperature, the final products from both synthesis methods were purified using the same protocol. The nanowire solutions were centrifuged at 10,000 rpm for 20 minutes, and the pellet was subsequently washed twice with water and centrifuged again at the same rate and time. Finally, the precipitate was resuspended in 35 mL of deionized water. The resulting solution containing the nanowires was transferred into a 20-mL glass vial, which was then placed in a freezer at −80°C for 4 hours and lyophilized overnight. The final powder was weighed and resuspended in a suitable amount of deionized and autoclaved water to reach the final concentration needed for further experiments.

## Instruments and characterization

A Heratherm™ General Protocol Oven (Thermo Fisher Scientific, Waltham, MA, USA) was used to produce the hydrothermal reaction in both chemical synthetic and green methodologies. An Eppendorf™ Model 5804-R Centrifuge was used for the centrifugation of the samples. A FreeZone Plus 2.5-L Cascade Console Freeze Dry System was used to purify the samples and to obtain the final TeNW structures.

TeNWs prepared by both chemical synthetic and green approaches were properly characterized using a JEM-1010 transmission electron microscope (JEOL USA Inc., Peabody, MA, USA). For sample preparation, purified nanostructures were air-dried on 300-mesh copper-coated carbon grids (Electron Microscopy Sciences, Hatfield, PA, USA). The samples were then imaged up to an 80,000× magnification with an accelerating voltage of 80.0 kV.

EDX spectroscopy analysis was performed using a dedicated EDX detector coupled with a Hitachi S-4800 scanning electron microscope. TeNW samples were affixed to 300-mesh copper-coated carbon grids and placed into an aluminum pin mount. An accelerating voltage of 10.0 kV was used to obtain an elemental spectrum for the NPs.

FT-IR spectra were recorded using a PerkinElmer Spectrum 400 FT-IR/FT-near infrared in attenuated total reflectance mode. For FT-IR spectroscopy measurements, 5 µg of the dried sample was used.

Powder XRD patterns were obtained using a Rigaku Miniflex 600 (Rigaku Co. Tokyo, Japan) operating at a voltage of 40 kV, a current of 15 mA, and a Cu-Kα radiation of 1.542 Å. All XRD patterns were recorded at a room temperature with a step width of 0.05 (2) and a scan speed of 0.2°/min. The samples were used from the powder obtained after the purification process.

In the XPS, drops of both compounds dispersed in water were deposited on clean copper substrates for sample preparation. After water evaporation, the samples were loaded in a vacuum load lock chamber and then transferred to the XPS ultra-high vacuum chamber with a base pressure of $10^{-10}$ mbar. The XPS chamber is equipped with a hemispherical electron energy analyzer (SPECS Phoibos 100 spectrometer, Berlin, Germany) and an Mg-Kα (1,253.6 eV) X-ray source. The angle between the hemispherical analyzer and the plane of the surface was kept at 60°. Wide scan spectra were recorded using an energy step of 0.5 eV and a pass energy of 40 eV, while specific core level spectra (Te 3d, O 1s, and C 1s) were recorded using an energy step of 0.1 eV and a pass energy of 20 eV. The absolute binding energies of the photoelectron spectra were determined by referencing to the Te 3d 5/2 metallic core level at 573 eV.[63] Data processing was performed with CasaXPS software (Casa software Ltd., Cheshire, UK). The contributions of the Mg-Kα satellite lines were subtracted.

Optical microscopy analysis was done on a phase contrast mode using an Axio Observer Z1 Inverted Fluorescence Microscope (Carl Zeiss, Oberkochen, Germany). For sample preparation, cells were grown on a 6-well plate with the presence of different GREEN-TeNWs and CHEM-TeNWs for 1, 3, and 5 days. Images were taken at these time points.

## In vitro cytotoxicity assays with TeNWs

Cytotoxicity assays were performed with primary HDF cells (human skin fibroblast/human skin cells, strain CCL-110; American Type Culture Collection® [ATCC®], Manassas, VA, USA) and human melanoma cells (Human Malignant Melanoma (A375), strain CRL-1619; ATCC®). The cells were cultured in DMEM (Thermo Fisher Scientific), supplemented with 10% FBS (ATCC® 30–2020™) and 1% penicillin/streptomycin (Thermo Fisher Scientific). MTS assays (CellTiter 96® Aqueous One Solution Cell Proliferation Assay; Promega, Madison, WI, USA) were carried out to assess cytotoxicity. The cells were seeded onto tissue-culture-treated 96-well plates (Thermo Fisher Scientific) at a final concentration of 5,000 cells per well in 100 µL of cell culture medium. An incubation period of 24 hours at 37°C in a humidified incubator with 5% carbon dioxide was employed. The culture medium was then replaced with 100 µL of fresh cell culture medium containing concentrations from 5 to 100 µg/mL of either CHEM-TeNWs or GREEN-TeNWs.

The cells were cultured for three different periods of time to compare the effects of the nanostructures on the cells after days 1, 3, and 5 following exposure.

The cells were washed with PBS, and the original media were replaced with 100 µL of the MTS solution (prepared using a mixing ratio of 1:5 of MTS/medium). After the addition of the solution, the 96-well plate was incubated for 4 hours in the incubator to allow for a color change. Then, the absorbance was measured at 490 nm on an absorbance plate reader (SpectraMAX® M3; Molecular Devices, San Jose, CA) for cell viability after exposure to the TeNWs. Cell viability was calculated by dividing the average absorbance obtained for each sample by that of the control sample and then multiplied by 100. Controls containing cells and media, only media and nanowires in media, were also added in the 96-well plate to identify the healthy growth of cells without nanowires and to determine the absorbance of both the media and the nanowires.

## Statistical analysis

All experiments were repeated in triplicate (N=3) to ensure the reliability of the results. Statistical significance was assessed using Student's *t*-tests, with $P<0.05$ being statistically significant. The results are displayed as mean ± SD.

# Results and discussion

## Synthesis of green biogenic TeNWs

The hydrothermal synthesis of TeNWs was successfully completed using both chemical and green synthesis protocols. Table 1 shows the comparison between the methods.

One of the most remarkable differences between the two synthesis methods is the relative cost and quantity of the reducing agents needed to reduce ionic Te to elemental Te. On one hand, CHEM-TeNWs were generated in an aqueous solution with the presence of two reducing agents (hydrazine and $NH_3$) and PVP as stabilizing and structure-directing agent. Liu et al[64] found that PVP has a steric effect

**Table 1** Synthesis conditions of the protocols used to prepare TeNWs

| Reaction features | CHEM-TeNWs | GREEN-TeNWs |
|---|---|---|
| Reducing agents | $NH_3/N_2H_4$ | Starch |
| Conditions | 180°C/4 hours | 160°C/15 hours |

**Abbreviations:** CHEM-TeNWs, chemically synthesized TeNWs; GREEN-TeNWs, green-synthesized TeNWs; TeNWs, tellurium nanowires.

on the growth of Te along the [0001] direction. On the other hand, GREEN-TeNWs were generated under the action of starch as unique reducing and stabilizing agent, which makes the synthetic approach cheaper and more environmentally-friendly that the one followed for the production of CHEM-TeNWs.

In the chemical synthesis, using hydrazine and $NH_3$ raises a huge safety concern when performing this process, as both are flammable, extremely toxic, and hazardous. Hydrazine in particular produces explosive vapors/air mixtures at about 38°C. Besides, it is corrosive to metals and skin and a real threat to the environment. Face shields and full-face respirators are needed to work with this chemical. PVP is however a water-soluble polymer that contributes to the formation of the nanostructures, and it is US Food and Drug Administration–approved.

On the other hand, the green synthetic approach needs only starch that is clearly a safe, naturally occurring reducing and stabilizing agent. This polymeric carbohydrate consists of a large number of glucose units that can reduce the Te ions to their elemental form. Therefore, because no additional agent is needed, this method holds advantages over the chemical synthesis method in terms of both cost and safety. Another concern to note is the production of toxic by-products. While waste produced from CHEM-TeNWs synthesis should be considered hazardous, the generation of reaction-derived products from the green synthesis process developed should not be viewed as an environmental threat.

Regarding the time for the reactions, the chemical synthesis of TeNWs took 4 hours at 160°C, while the green process took 15 hours at 180°C. This extra time can be explained by the reducing power of starch, which is lower than when using hydrazine and $NH_3$; however, considering the hazards of the chemicals and by-products of the chemical synthesis approach, the green methodology still has plenty of advantages such as being more economical and easy and following a straightforward hydrothermal synthesis method. Nevertheless, the green synthetic approach employed can be made quicker since the time used for the growth of the nanowires can be reduced to a couple of hours. It was hypothesized that the density of wires would be less than that using 15 hours; however, this is a hypothesis that needs further development.

Moreover, in the control experiment, a colorless solution was obtained in comparison with the dark one of both GREEN-TeNWs and CHEM-TeNWs (Figure 1) after the reaction process.

The control experiment was also characterized with TEM, and no nanostructures were found; therefore, no nanowires were obtained without the use of starch. Consequently, the role of starch is crucial to reduce the metal and obtain the nanostructures.

**Figure 1** Solutions of GREEN-TeNWs after the reaction. The colorless solution without starch (left) and dark solution containing starch (right).
**Abbreviation:** GREEN-TeNWs, green-synthesized tellurium nanowires.

## Characterization

Morphological characterization was completed for both of the synthesis approaches with size and coating characteristics reported in Table 2.

Specifically, CHEM-TeNWs (Figure 2A and B) had an average diameter of 30 nm with a length of several micrometers. The wires showed a low degree of aggregation. On the other hand, GREEN-TeNWs (Figure 2C and D) showed an average diameter of about 20 nm with a similar length. The peculiarity of these structures was due to their morphology. It seemed that nanowires started growing from a particular point, and they extended as far as they could. The main trunk was divided into several smaller sections at the end of the structure as ramifications, which produced branches that grew alongside one another.

SEM characterization was performed on the GREEN-TeNWs (Figure 3C and D). The wires started growing from a cluster and extended for several micrometers, with a star-shaped uniform structure that was difficult to observe when the clusters were close to one another.

**Table 2** Data from transmission electron microscopy for size and coating

| Structures | CHEM-TeNWs | GREEN-TeNWs |
|---|---|---|
| Length | Several microns | Several microns |
| Width | 32±11 nm | 25±8 nm |
| Coating | No | Yes |

**Abbreviations:** CHEM-TeNWs, chemically synthesized TeNWs; GREEN-TeNWs, green-synthesized TeNWs; TeNWs, tellurium nanowires.

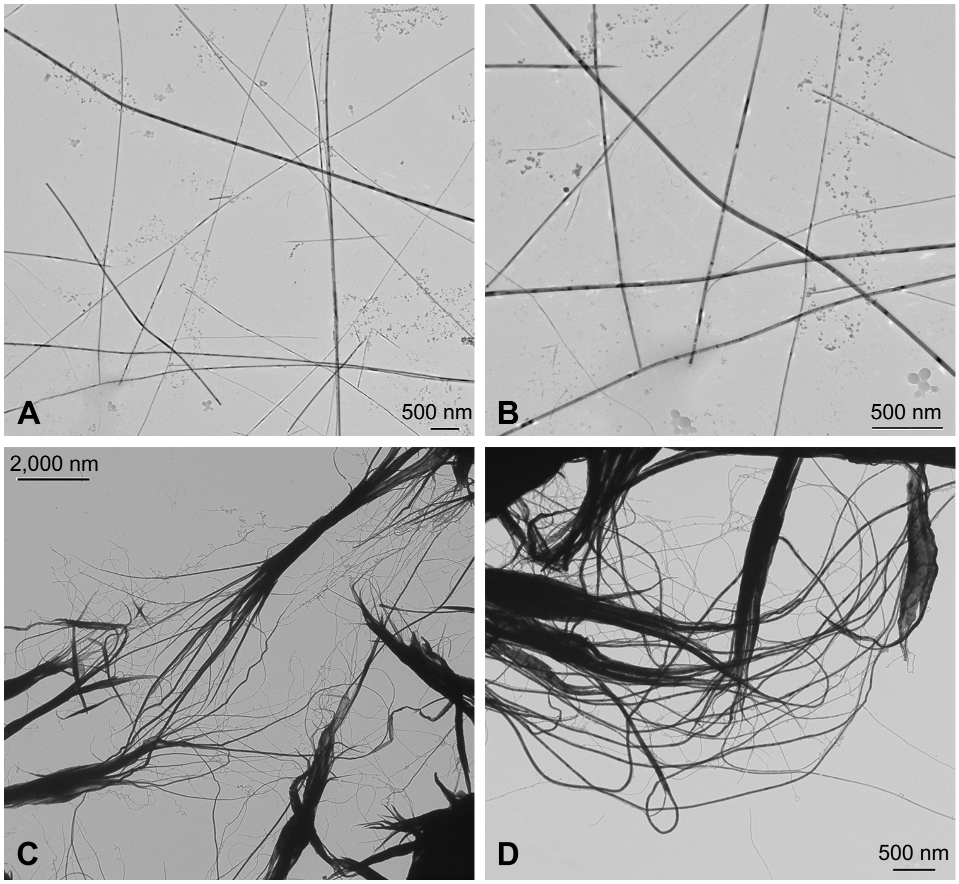


**Figure 2** Transmission electron microscopy images of TeNWs. CHEM-TeNWs with a low degree of aggregation were found dispersed within the solution (**A**) and (**B**). GREEN-TeNWs (**C** and **D**) showed a higher degree of aggregation, and the presence of an organic coating was observed.
**Abbreviations:** CHEM-TeNWs, chemically synthesized TeNWs; GREEN-TeNWs, green-synthesized TeNWs; TeNWs, tellurium nanowires.

When CHEM-TeNWs were observed, the structures were found to grow on the top of each other generating a cluster that could affect cell viability (Figure 3A). Besides, different morphologies (Figure 3B) – crystals, nanowires (NWs) with variable widths and irregular structures – were found in solution which can lead to potential distinct performance regarding their biomedical applications.

It has been hypothesized that the differences between both structures came from the presence of starch. This polymer is known to have ramifications, and it has been elucidated that TeNW grow following the template of starch. Moreover, the uniformity of the GREEN-TeNWs morphology is thought to enhance their action in anticancer and biocompatibility properties in comparison with the chemically synthesized products.

EDX spectroscopy measurements were completed for both the chemically synthesized and green-synthesized nanostructures. For CHEM-TeNWs (Figure 4A), EDX spectroscopy analysis showed that the electron-dense nanowires had specific Te absorption peaks. For GREEN-TeNWs, the peaks for Te were higher due to the higher concentration of Te within the sample (Figure 4B). When the analysis focused on the surrounding areas of the nanostructures, the carbon peak was significantly raised compared with the measurement of the Te metallic core. This, aside from the absence of a Te peak, indicated an organic composition of the coating (Figure 4C).

In Figure 5, we compare the FT-IR spectra of CHEM-TeNWs, GREEN-TeNWs, and potato starch. The CHEM-TeNWs and GREEN-TeNWs samples show absorption bands of Te oxide at around 765 and 585 $cm^{-1}$, which can be related to the symmetrical equatorial and asymmetrical axial stretching frequencies of the Te–O bond, respectively.[65,66] The FT-IR spectrum of GREEN-TeNWs presents a vibrational band at around 3,300 $cm^{-1}$ related to the O–H stretching mode of starch. The vibrational bands at the region of 1,300–1,400 $cm^{-1}$ are due to C–O–H bending and $CH_2$ twisting of the starch structure.[67]

Figure 6 shows the XRD patterns for CHEM-TeNWs and GREEN-TeNWs. Practically, all the diffraction peaks in both experimental XRD patterns can be indexed to hexagonal Te structure (*h*-Te, space group P3121).[68] The lattice parameters calculated for both the samples are in good

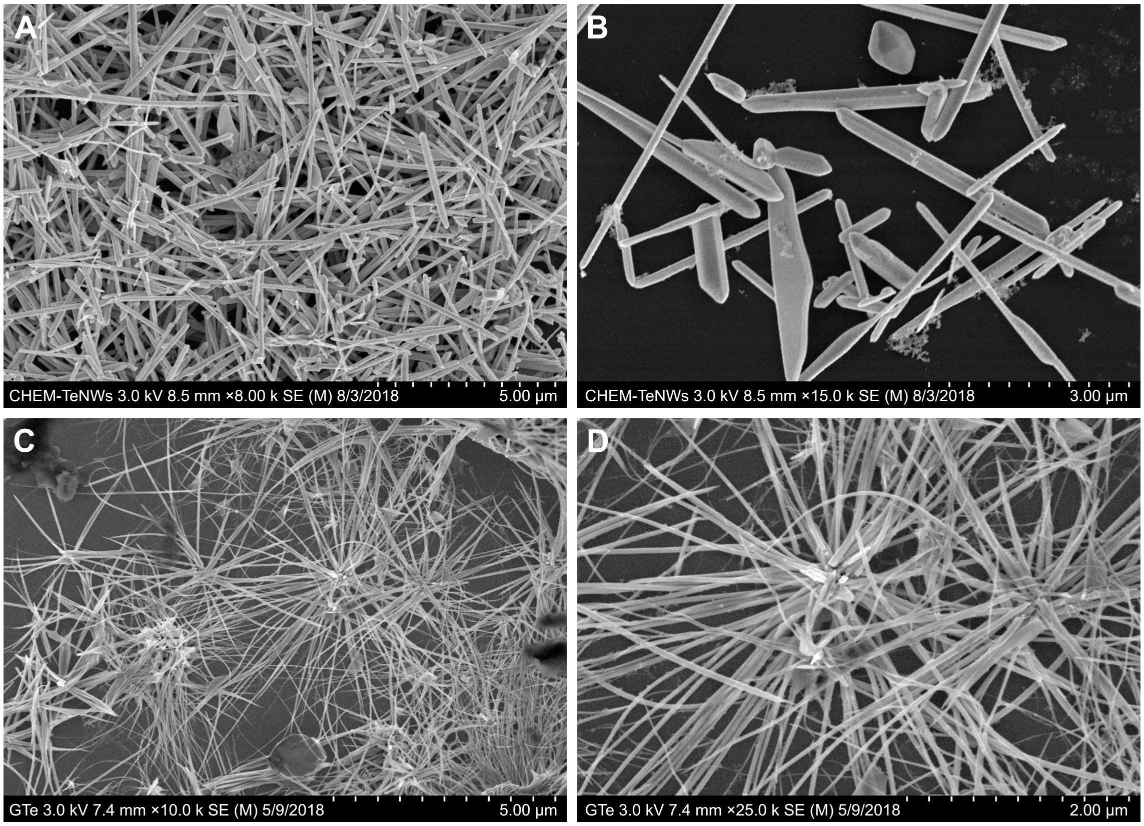


**Figure 3** SEM images of CHEM-TeNWs (**A** and **B**) and GREEN-TeNWs (**C** and **D**). GREEN-TeNWs grew with a star-shaped structure, while CHEM-TeNWs had different morphologies.

**Abbreviations:** CHEM-TeNWs, chemically synthesized TeNWs; GREEN-TeNWs, green-synthesized TeNWs; SEM, scanning electron microscopy; TeNWs, tellurium nanowires.

agreement with the reported values for *h*-Te,[68] as shown in Table 3. In the case of the XRD pattern of GREEN-TeNWs the presence of foreign phases related to Te-based oxides compounds were also detected (Figure 6).

For CHEM-TeNWs, three different phases were identified corresponding to elemental Te, sodium tellurate hydrate, and an organic compound. This last one was present on a relatively little amount compared with the other ones; it has

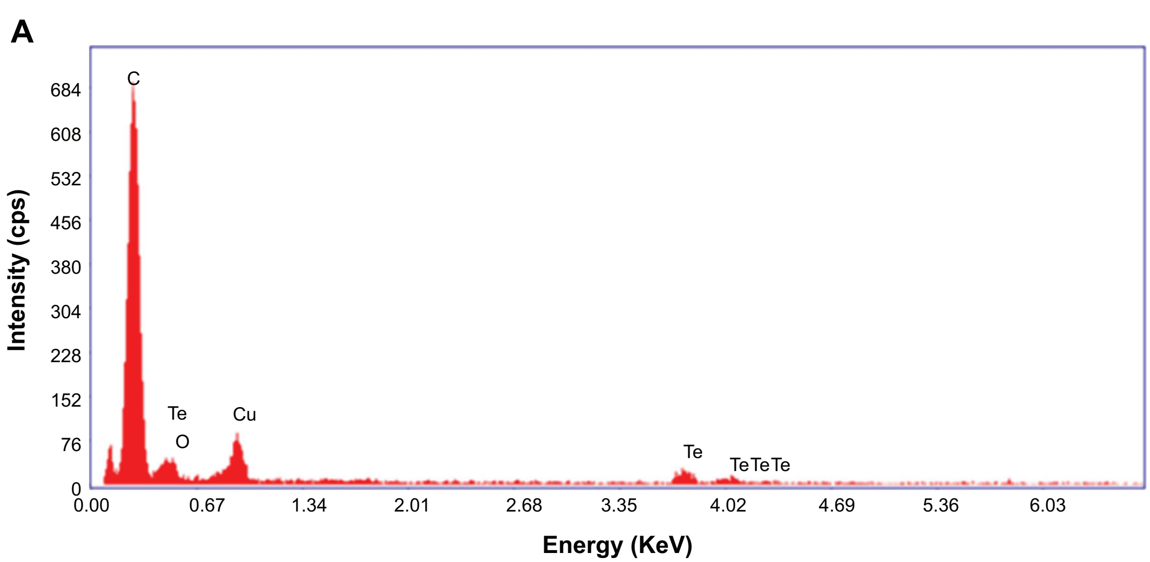


**Figure 4** (*Continued*)

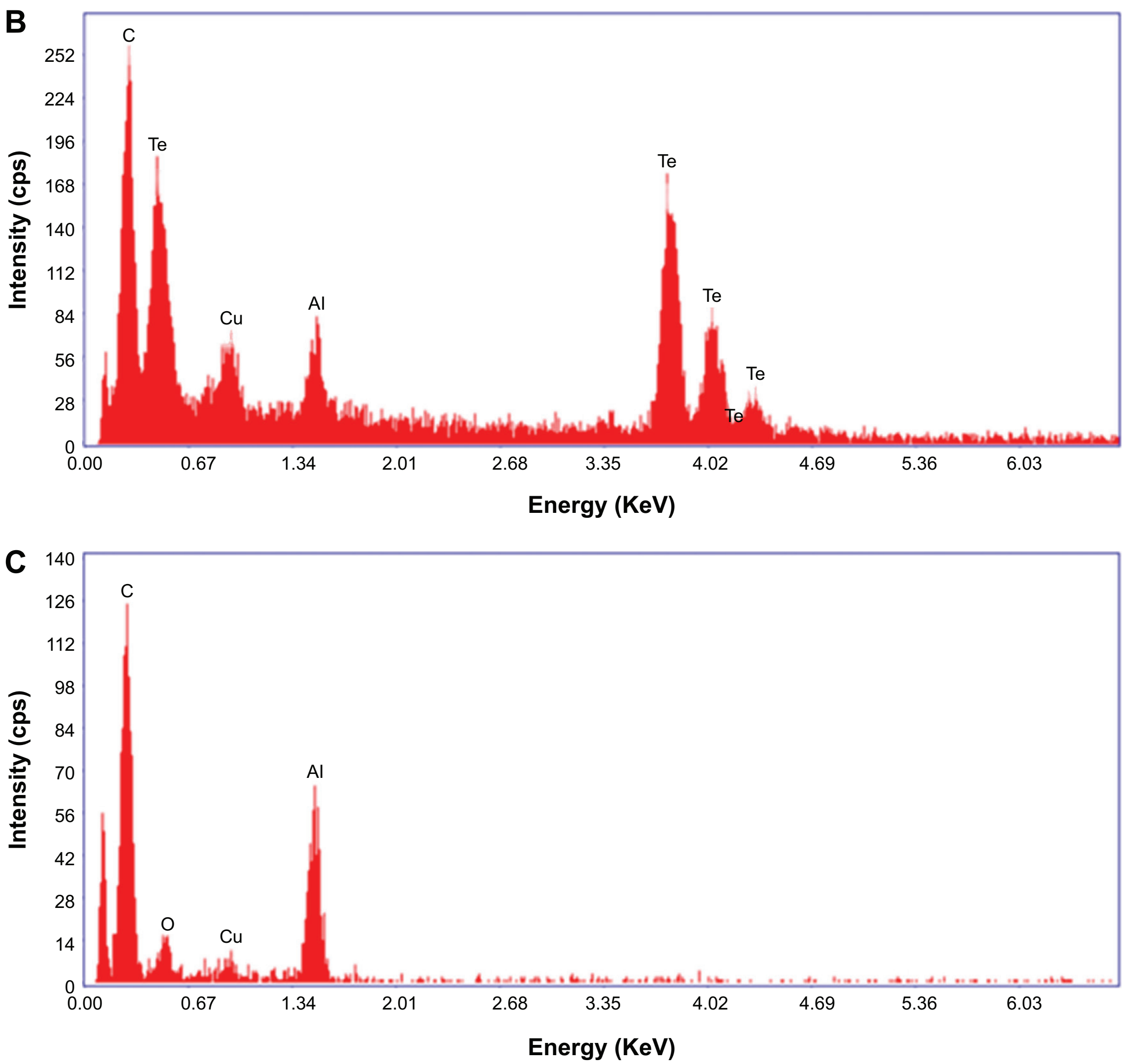


**Figure 4** Energy-dispersive X-ray of TeNWs. CHEM-TeNWs were characterized (**A**) as well as GREEN-TeNWs in both the metallic core (**B**) and the surrounding coating (**C**).
**Abbreviations:** CHEM-TeNWs, chemically synthesized TeNWs; GREEN-TeNWs, green-synthesized TeNWs; TeNWs, tellurium nanowires.

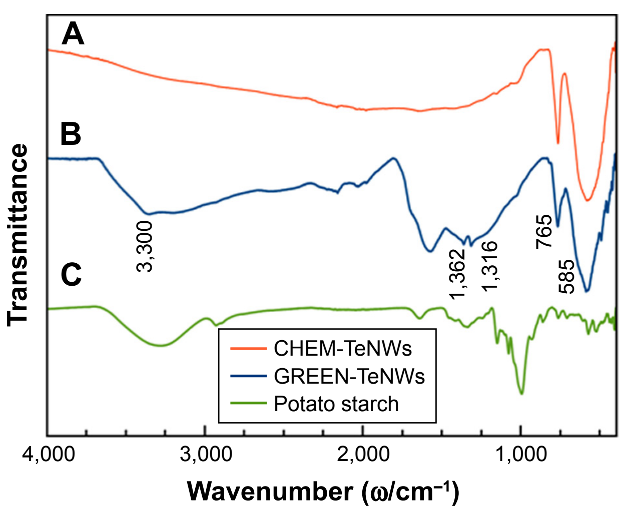


**Figure 5** FT-IR spectra of (**A**) CHEM-TeNWs, (**B**) GREEN-TeNWs, and (**C**) potato starch.
**Abbreviations:** CHEM-TeNWs, chemically synthesized TeNWs; FI-TR spectra, Fourier-transform infrared spectra; GREEN-TeNWs, green-synthesized TeNWs; TeNWs, tellurium nanowires.

been hypothesized that its presence came from a hydrocarbon-based deposition of organic matter on the top of the sample either after the purification or after the preparation of the sample. On the other hand, GREEN-TeNWs present elemental Te, Te oxide, and organic compound phases. The presence of Te oxide has been related to the use of starch as a reducing agent as oxygen was integrated into the structure. It has been elucidated that the organic compound was associated with the use of starch. Additional information can be find in Supplementary Material (Figures S1–S4 and Tables S1–S4).

XPS was used to characterize the chemical composition and electronic states of both CHEM-TeNWs and GREEN-TeNWs.

Figure 7 displays the wide scans that have been normalized arbitrarily to the C 1s core level peak for comparison. The main features have been identified in the spectra.

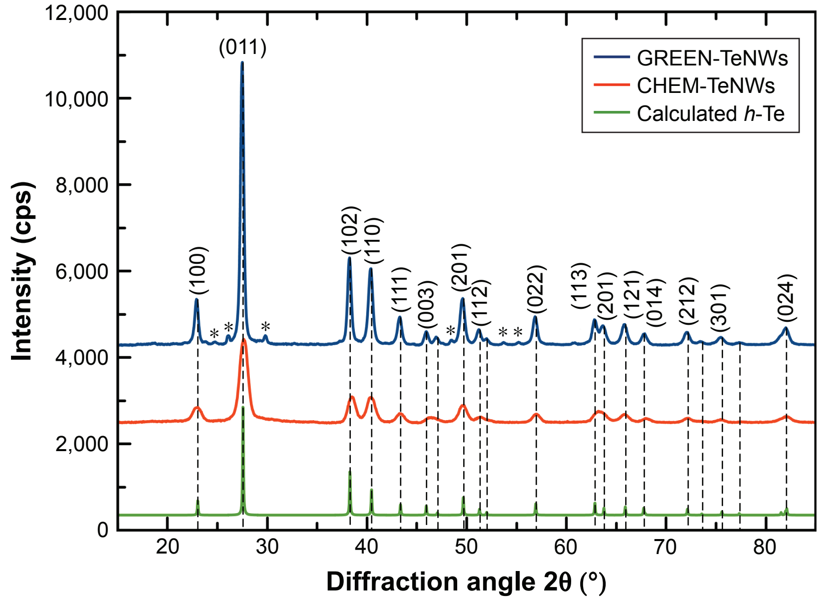


**Figure 6** Comparison between the experimental XRD patterns for GREEN-TeNWs and CHEM-TeNWs and the calculated XRD patterns for bulk hexagonal Te (*h*-Te).[68] The diffraction peaks marked with (*) may be related to Te-based oxides.

**Abbreviations:** CHEM-TeNWs, chemically synthesized TeNWs; GREEN-TeNWs, green-synthesized TeNWs; TeNWs, tellurium nanowires; XRD, X-ray powder diffraction.

Clear differences can be observed between the two compounds. As the spectra are normalized to the C 1s core level peak, the higher intensity at the Te 3d core level for CHEM-TeNWs indicates that this compound has a higher content of Te than that in GREEN-TeNWs. In addition, the double structure for the Te 3d core level peaks (CHEM-TeNWs) is likely to indicate that this element is partially oxidized. Finally, it clearly appears that GREEN-TeNWs have no nitrogen (absence of N 1s core level peak) as compared to the CHEM-TeNWs; these differences can be explained due to the use of hydrazine and $NH_3$ as reductor agents in the chemical synthetic approach.

The chemical analysis performed at the Te 3d, O 1s, N 1s, and C 1s core level peaks revealed the composition given in Table 4.

Differences between the two compounds are better appreciated when comparing the Te 3d core levels as shown in Figure 8. The spectra have been normalized to the Te $3d_{5/2}$ oxide component (at a binding energy of 576 eV) and shifted vertically for comparison.

**Table 3** Hexagonal lattice parameters calculated for GREEN-TeNWs and CHEM-TeNWs

| Sample | *a*/Å | *c*/Å |
|---|---|---|
| CHEM-TeNWs | 4.478 | 5.816 |
| GREEN-TeNWs | 4.484 | 5.915 |
| *h*-Te[68] | 4.456 | 5.921 |

**Abbreviations:** CHEM-TeNWs, chemically synthesized TeNWs; GREEN-TeNWs, green-synthesized TeNWs; *h*-Te, hexagonal Te; TeNWs, tellurium nanowires.

As can be observed, metallic and oxide components could clearly be identified. The metallic components are located at 573 eV (chosen as a reference in order to correct the charging effects) and 583.4 eV for the Te $3d_{5/2}$ and Te $3d_{3/2}$ peaks, respectively, whereas the oxide components are located at 576 eV and 586.6 eV for the Te $3d_{5/2}$ and Te $3d_{3/2}$ structures, respectively, which are in agreement with the previous results.[63,69] It also clearly appears that GREEN-TeNWs have more of a Te oxide (79%) component than the CHEM-TeNWs (61% oxide) as seen previously on the XRD results.

The two compounds also present differences at the C 1s and O 1s core levels (Figure 9).

The C 1s core levels spectra (Figure 9, left) could be fitted with the following minimum number of components at 281.1 eV (13%), 283.7 eV (71%), and 286.6 eV (16%) for GREEN-TeNWs and 285.1 eV (57%) and 286.8 eV (43%) for CHEM-TeNWs. The peaks located at 286.6 eV and 286.8 eV can be ascribed to hydroxyl (C–O/C–OH) groups,[70,71] meaning that CHEM-TeNWs have more hydroxyl groups than GREEN-TeNWs. At a lower binding energy, a peak located at 285.1 eV could be identified in CHEM-TeNWs. This peak corresponds to the presence of either C–C or C–H bonds in the $sp^3$ tetrahedral configuration,[71] and surprisingly, it was not observed in GREEN-TeNWs. Instead, two peaks at lower binding energies of 281.1 eV and 283.7 eV were identified on it. The peak at 283.7 eV could be ascribed to C–C bonds in the sp2 configuration, while the less abundant component with an XPS peak at 281.1 eV could not be clearly

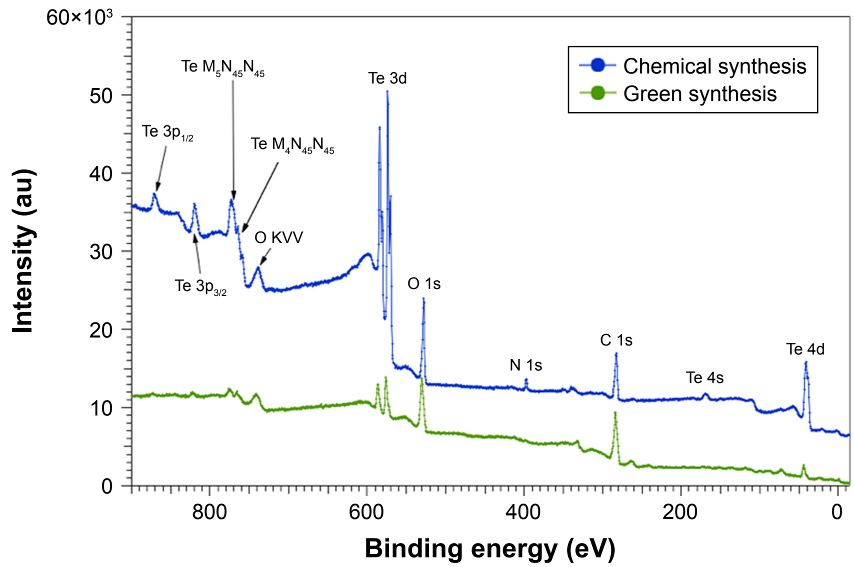


**Figure 7** Wide scans recorded on both compounds synthesized through the green and chemical routes.

identified. It is inferred that this last component corresponds to C atoms weakly bonded. Thus, no evidence of the presence of carbonyl (C=O at 288.1 eV) or carboxyl (O–C=O at 289.0 eV) groups could be observed.[71]

In the case of the O 1s core level spectra (Figure 9, right), the spectrum corresponding to GREEN-TeNWs could be fitted with a single component at 530 eV, while CHEM-TeNWs have two components located at 530.6 eV (44%) and 531.3 eV (56%). These relatively weak binding energies suggest that the oxygen atoms are weakly bonded and do not correspond to O–C bonds that would appear at a binding energy of around 533 eV.[70] This in turn agrees with the absence of carbonyl and carboxyl groups in the C 1s spectra.

## In vitro cytotoxicity of TeNWs

In vitro cytotoxicity assays were performed with HDF cells and melanoma cells (ATCC® CRL-1619). Data from the nanowire treatment were compared with a control that contained only cells and media. A comparison was made between HDF and melanoma cells with the aim of determining potential anticancer activity. The same experiments were performed using chemical and green-synthesized nanowires to determine the effect of the natural coating present on GREEN-TeNWs on the proliferation of the cells.

For HDF experiments, nanowires at a concentration between 5 and 100 µg/mL were tested. For CHEM-TeNWs, the same proliferation trend was observed within the third and fifth day for concentrations up to 15 µg/mL compared with the control (Figure 10A). However, the number of cells was less than that for the control in all the cases. Larger concentrations showed degeneration of the cell proliferation. When GREEN-TeNWs were tested on the cells, a similar proliferation trend was observed for each of the concentrations (Figure 10B). An especially unusual behavior was shown at levels between 15 and 75 µg/mL, with a higher number of

**Table 4** Chemical composition (in percentage atomic concentration) extracted from the Te 3d, O 1s, N 1s, and C 1s core level peaks

| | Green route | Chemical route |
|---|---|---|
| Tellurium | 2.6 | 17.1 |
| Oxygen | 67.8 | 31.5 |
| Nitrogen | – | 5.3 |
| Carbon | 29.6 | 46.1 |

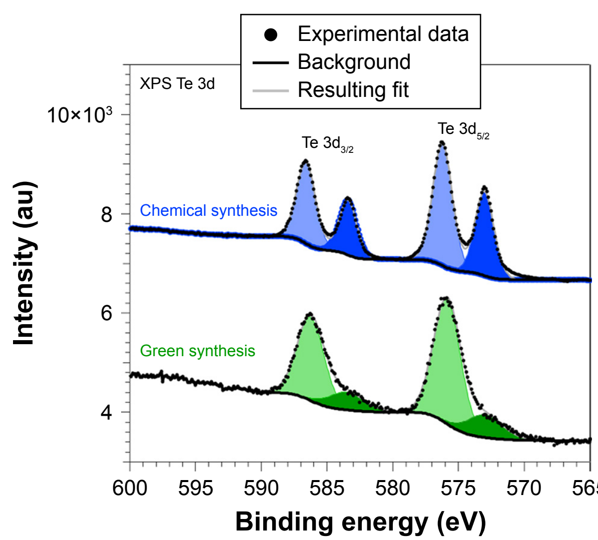


**Figure 8** XPS spectra recorded at the Te 3d core levels for samples synthesized through the chemical and green routes.
**Abbreviation:** XPS, X-ray photoelectron spectroscopy.

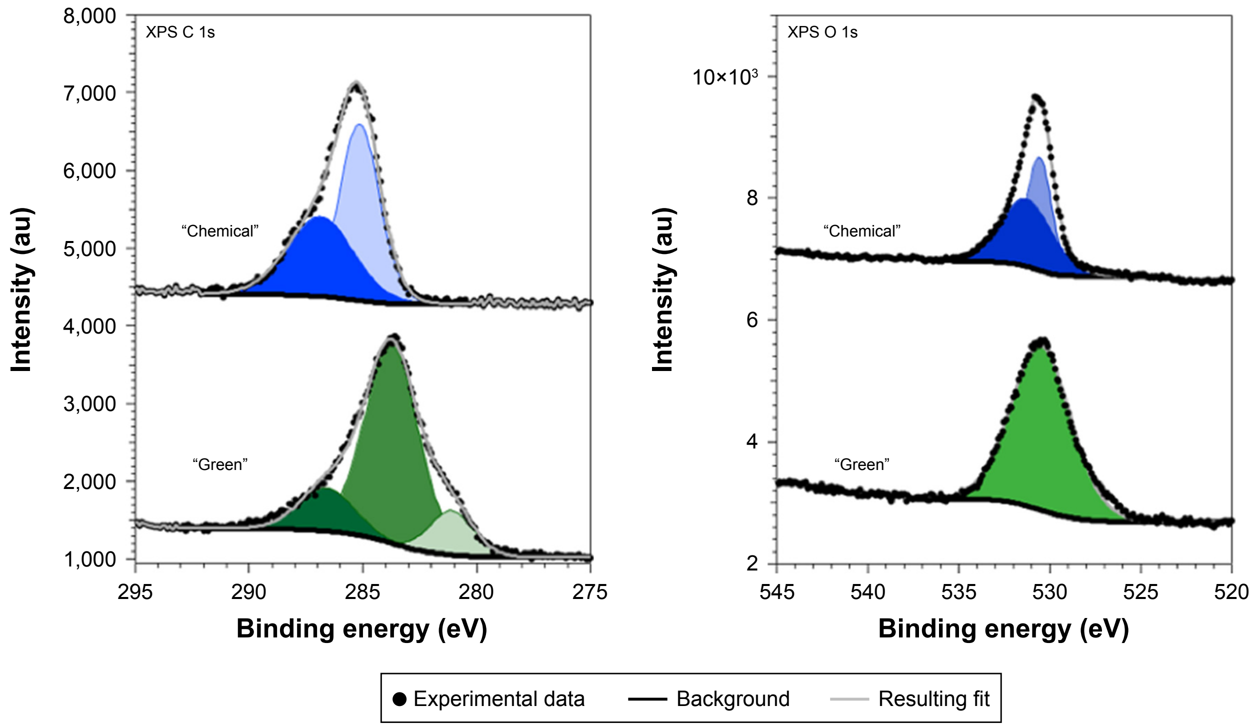


**Figure 9** XPS spectra recorded at the C 1s (left) and O 1s (right) core levels for samples synthesized through the chemical and green routes.
**Abbreviation:** XPS, X-ray photoelectron spectroscopy.

cells growing within the third and the fifth day compared with the first 24 hours. When both nanostructures were compared, it can be concluded that the green-synthesized structures enhanced cell proliferation over a broader range of concentrations compared with the chemical synthetic ones.

The cytotoxic effect of Te nanostructures is the result of active physicochemical interactions of elemental Te with the functional groups of intracellular proteins and the bases and phosphate groups in DNA.[60] While cytotoxicity was apparent for the CHEM-TeNWs (Figure 10A), we hypothesized that the enhanced biocompatibility in GREEN-TeNWs (Figure 10B) is most likely due to the presence of a natural, organic coating that encompasses the Te core. The presence of a carbon layer as the natural coating introduces a biodegradable material that can enhance cell proliferation.

When melanoma cells were treated with CHEM-TeNWs, cell proliferation showed a similar trend as that of the control at concentrations up to 25 µg/mL (Figure 10C). GREEN-TeNWs showed a similar behavior (Figure 10D). Nonetheless, levels between 10 and 100 µg/mL showed a delay in the cell proliferation compared with the control over the tested time period. It has been hypothesized that TeNWs have the potential ability to slow down the signaling processes present in cancerous cells due to the effect of Te.[72,73] Therefore, we propose that both synthesis methods produce nanostructures with anticancer properties, but specifically this behavior was particularly enhanced in the case of the green synthetic structures.

In this report, the cytocompatibility and anticancer activity of Te nanostructures were observed with a potentially improved performance using GREEN-TeNWs. Thus, not only were the GREEN-TeNWs produced with significantly fewer toxic materials, but their properties toward enhancing healthy cell proliferation and decreasing cancer cell proliferation were also greater.

A comparison was done on the fifth day of the experiments between samples to show the tendency of both cell compatibilities with HDF cells (Figure 11A) and cytotoxic effects with melanoma cells (Figure 11B).

The low cytotoxicity for HDF cells can be appreciated especially at high concentrations of TeNWs, with a noticeable difference between CHEM-TeNWs – with higher cytotoxicity for HDF – and GREEN-TeNWs, which allow for a high cell proliferation. At low concentrations – between 5 and 15 µg/mL – the difference in terms of biocompatibility was almost inappreciable. The biggest difference was observed at a concentration of 25 µg/mL. For experiments with cancerous cells, the opposite behavior occurred. GREEN-TeNWs did not allow for the proliferation of melanoma cells at concentrations ranging between 15 and 100 µg/mL. As with HDF cells, the bigger difference was observed for a concentration of

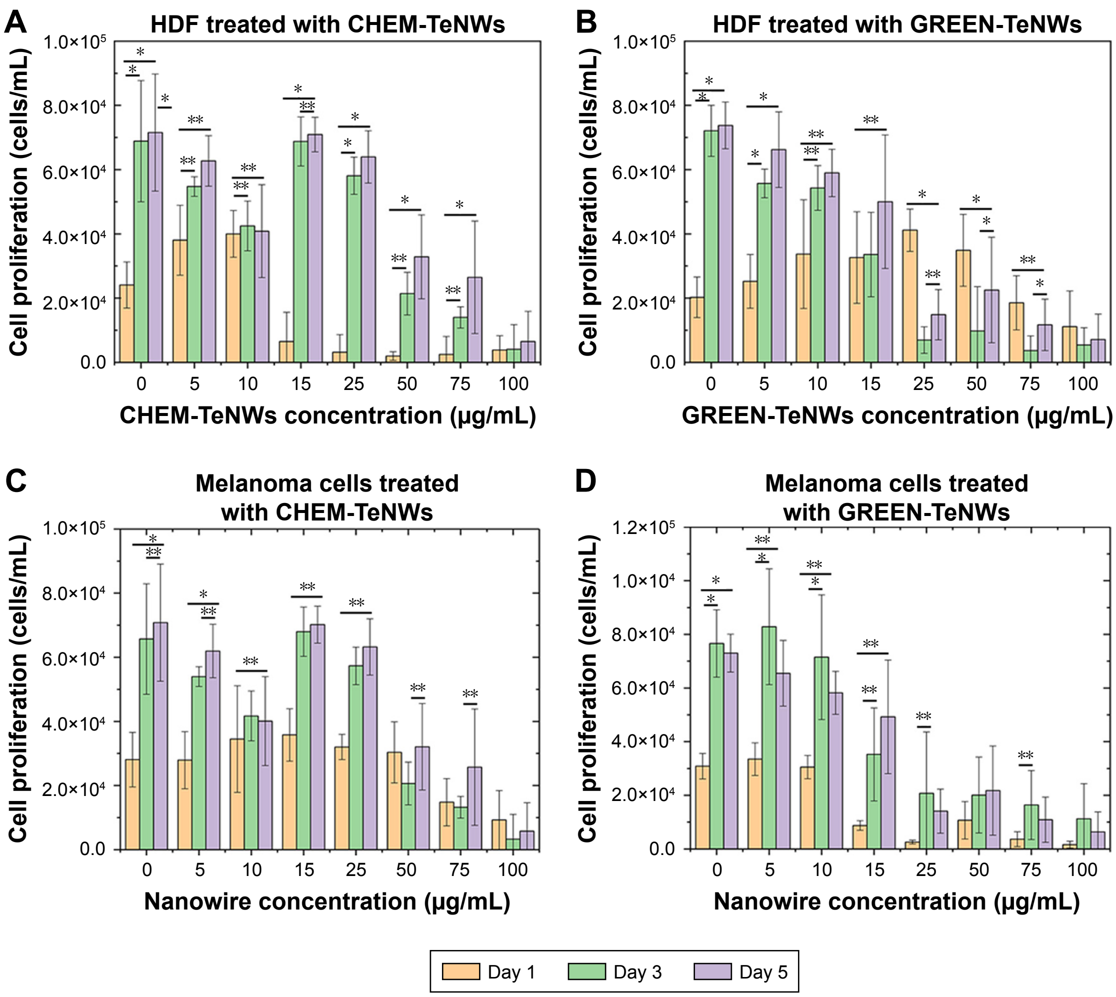


**Figure 10** MTS assays on HDF (**A**, **B**) and melanoma (**C**, **D**) cells in the presence of CHEM-TeNWs (**A**, **C**) and GREEN-TeNWs (**B**, **D**) at concentrations ranging from 5 to 100 µg/mL. N=3. Data are presented as mean ± SD; *$P<0.01$, **$P<0.005$.

**Abbreviations:** CHEM-TeNWs, chemically synthesized TeNWs; GREEN-TeNWs, green-synthesized TeNWs; HDF, human dermal fibroblasts; TeNWs, tellurium nanowires.

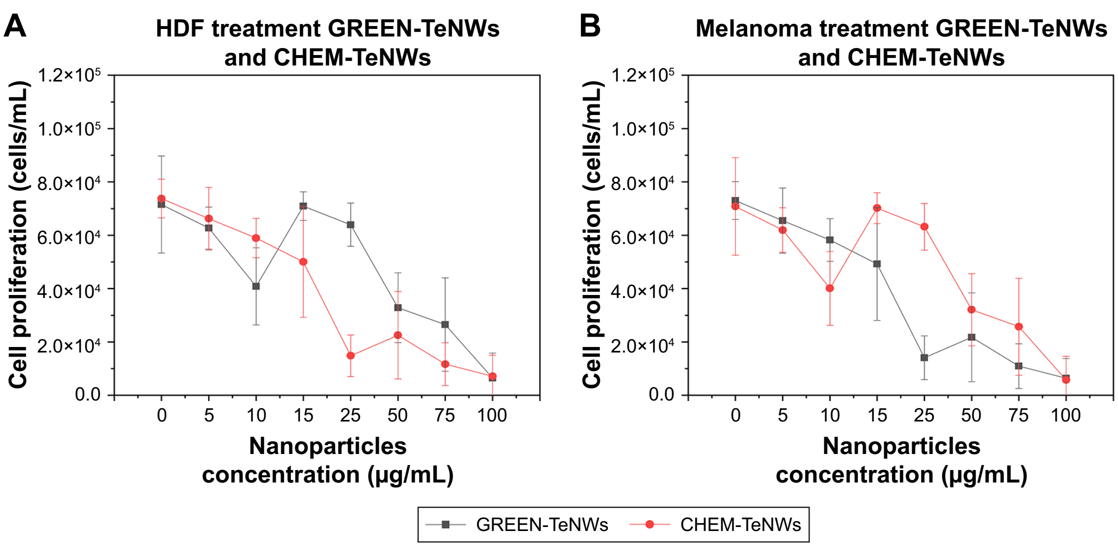


**Figure 11** Comparison between CHEM-TeNWs and GREEN-TeNWs for HDF (**A**) and melanoma (**B**) cells at the fifth day of experiment. Data from MTS assays on HDF and melanoma cells in the presence of TeNWs.

**Abbreviations:** CHEM-TeNWs, chemically synthesized TeNWs; GREEN-TeNWs, green-synthesized TeNWs; HDF, human dermal fibroblasts; TeNWs, tellurium nanowires.

**Table 5** $IC_{50}$ values for both CHEM-TeNWs and GREEN-TeNWs in experimental assays with HDF and melanoma cells after 5 days of experiments

| Cell assay | CHEM-TeNWs | GREEN-TeNWs |
|---|---|---|
| HDF | 60.22±15.25 μg/mL | 70.05±10.58 μg/mL |
| Melanoma | 63.14±6.078 μg/mL | 16.46±1.96 μg/mL |

**Abbreviations:** CHEM-TeNWs, chemically synthesized TeNWs; GREEN-TeNWs, green-synthesized TeNWs; HDF, human dermal fibroblasts; TeNWs, tellurium nanowires.

25 μg/mL. Therefore, it was possible to hypothesize that at a concentration of 25 μg/mL of GREEN-TeNWs, both the maximum biocompatibility for HDF and the maximum cytotoxic effect for melanoma cells were achieved in comparison with the same concentration of CHEM-TeNWs. As a general view, the behavior of GREEN-TeNWs after 5 days in terms of low and high cytotoxicity for HDF and melanoma cells, was enhanced in comparison with CHEM-TeNWs.

$IC_{50}$ values were calculated for all the experiments in Table 5, with the aim of showing the minimum inhibitory concentration for both HDF and melanoma cells. This value was obtained after 5 days of experiments, measuring the potency of the nanowires to inhibit the normal biological functioning of the cells.

The interaction between the cells and the nanostructures was studied using SEM imaging of melanoma and HDF cells. Different concentrations – 100, 50, and 0 μg/mL – of TeNWs were tested in order to elucidate the mechanism of cell death on both cell types. SEM imaging allowed the observation of modifications in the membrane and shape of cells.

For HDF cells, NWs were found to be in contact with the cells; however, no interaction between them was observed at lower concentrations. GREEN-TeNWs surrounded the cells without producing any damage (Figure 12A and B) when compared to the control (Figure 12C). The membrane remained intact without any sign of swelling or blebbing. Thus, it has been hypothesized that the presence of starch encores the TeNWs and prevents their interaction with HDF cells.

Nevertheless, higher concentrations of 100 μg/mL NPs seem to produce necrosis on cells (Figure 12D). As shown in

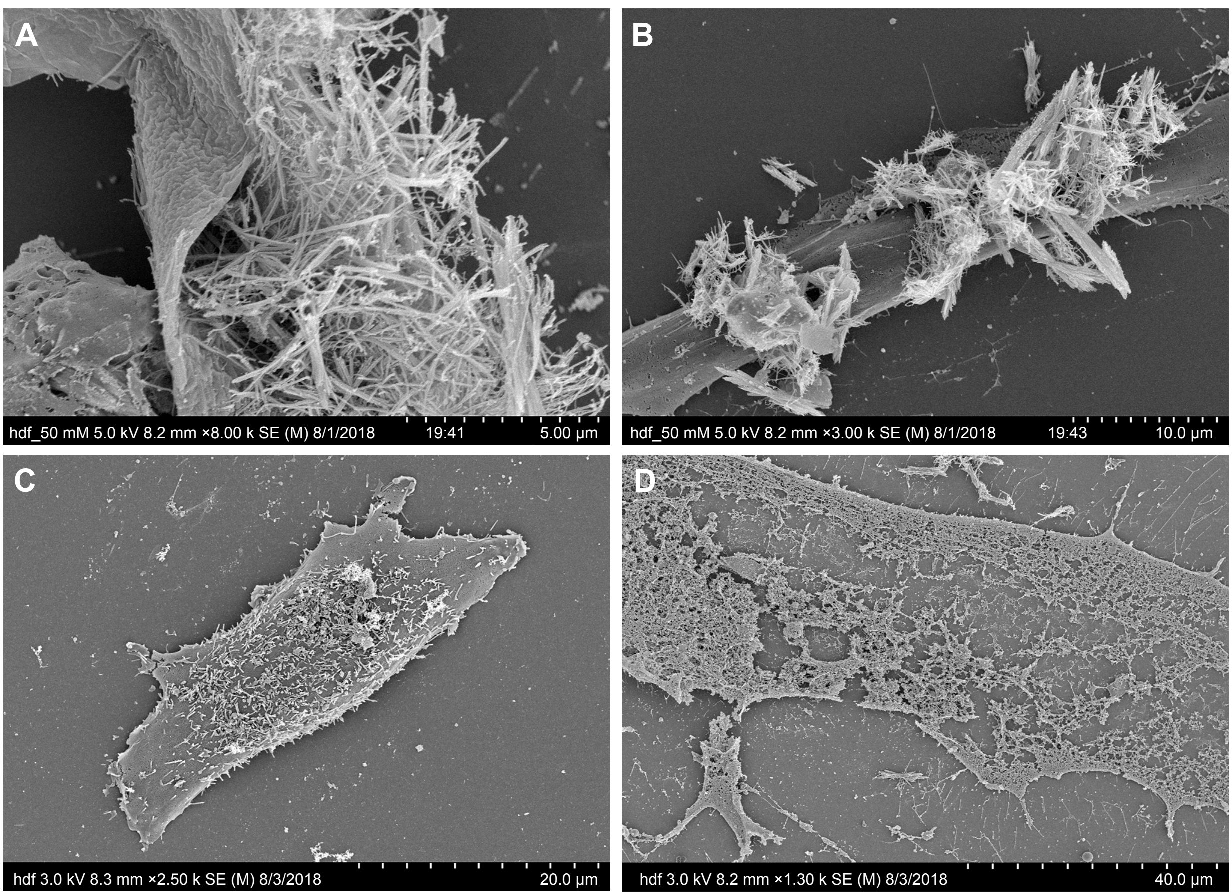


**Figure 12** Interaction between HDF cells and GREEN-TeNWs. Interaction between 50 μg/mL (**A**, **B**), 0 μg/mL (**C**), and 100 μg/mL (**D**) of GREEN-TeNWs and HDF cells was analyzed.

**Abbreviations:** GREEN-TeNWs, green-synthesized TeNWs; HDF, human dermal fibroblasts; TeNWs, tellurium nanowires.

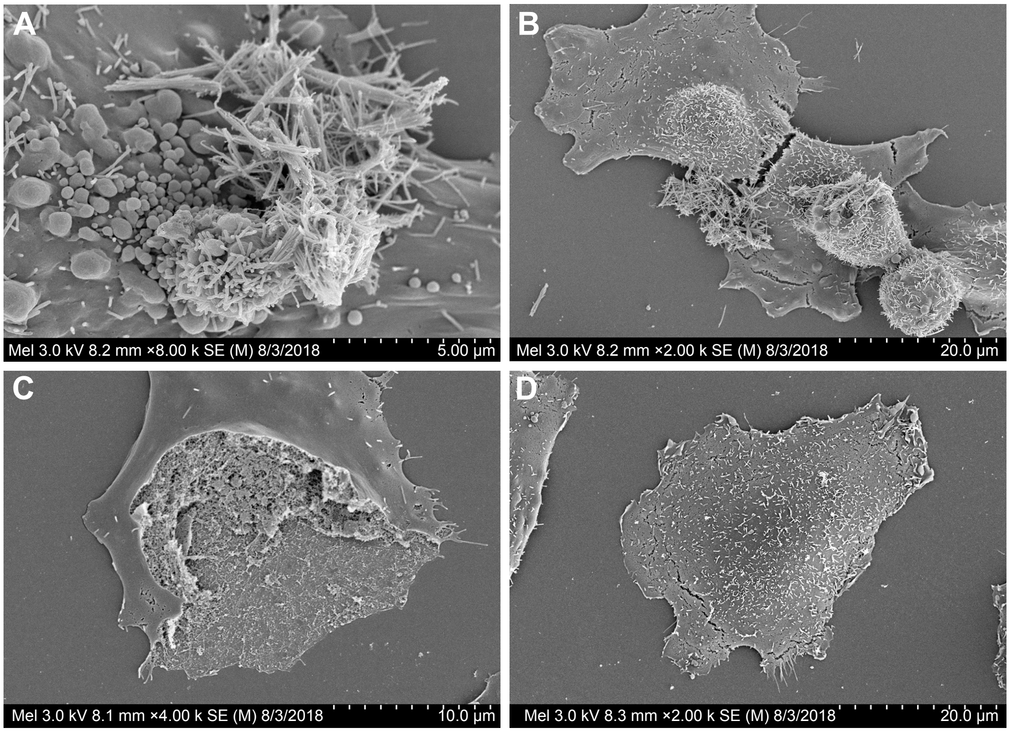


**Figure 13** Interaction between melanoma cells and GREEN-TeNWs. Bubbling (**A**) and rupture (**B** and **C**) of the cell membrane were observed in comparison with the control (**D**).
**Abbreviation:** GREEN-TeNWs, green-synthesized tellurium nanowires.

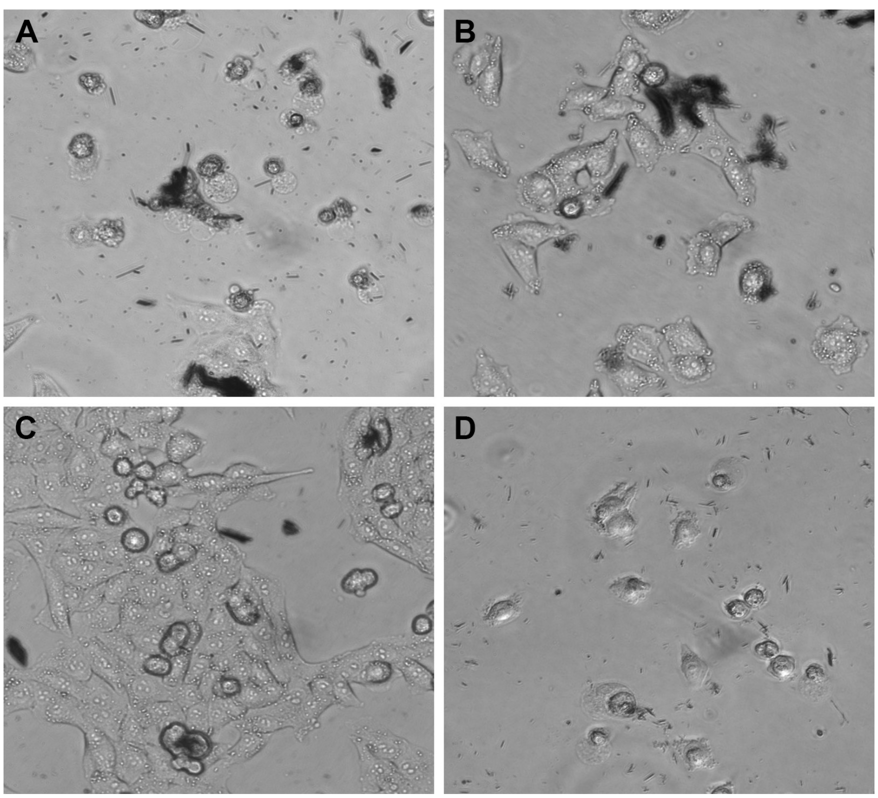


**Figure 14** Optical microscopy characterization of HDF (**A**, **B**) and human melanoma (**C**, **D**) cells cultured in the presence of both CHEM-TeNWs and GREEN-TeNWs for 24 hours.
**Abbreviations:** CHEM-TeNWs, chemically synthesized TeNWs; GREEN-TeNWs, green-synthesized TeNWs; HDF, human dermal fibroblasts; TeNWs, tellurium nanowires.

the literature, swelling of the cell due to a hydration process and discontinuities on the membrane previous to its rupture are dictated as signs of necrosis.[74,75] SEM captured the different stages of the rupture of the cytoplasmic membrane due to a swelling process (Figure 12D); hence, the mechanism of death was interpreted as necrosis.

In contrast, blebbing (Figure 13A) was observed on melanoma cells in comparison with the control (Figure 13D), indicating a process of apoptosis. These formations on the membrane are associated with a rearrangement in the cytoskeleton, which eventually ended in the rupture in fragments of the cell.[76,77] It has been hypothesized that differently than HDF, NWs interact with melanoma cells by inducing chemical signaling, which leads to apoptosis, hence reducing cell proliferation by breaking cells apart (Figure 13B and C). It has been elucidated that different mechanisms of death are possible due to the use of different kinds of cells.

Optical microscopy showed preliminary results of how different cells behaved in the presence of both GREEN-TeNWs and CHEM-TeNWs. After 24 hours of treatment, 50 μg/mL CHEM-TeNWs (Figure 14A) showed a remarkable disturbance in the growth of HDF cells after 24 hours of treatment, with poor cell development, while the same concentration of GREEN-TeNWs (Figure 14B) allowed the development of the cells to a large extent. When melanoma human cells were tested with the same concentration of CHEM-TeNWs (Figure 14C), the cells showed better development than the ones cultured with GREEN-TeNWs (Figure 14D) for the same period.

## Conclusion

Nanotechnology has taken an advantage of traditional chemical synthesis methods, both physical and chemical, to solve many of the biomedical and technological challenges that society faces today. Nevertheless, there is an environmental impact associated with such synthesis. Concerns such as the production of toxic by-products and harsh reaction conditions should be addressed. Therefore, new and alternative approaches are on the rise. One of the most promising comes from the use of green chemistry.

In this work, we successfully explored and compared two different synthesis approaches (a traditional chemical method and a green chemistry method) to elucidate the differences between the cytocompatibility and anticancer behavior of the respective NPs produced from each process. Experiments with healthy fibroblasts and cancerous melanoma cells were performed over a range of concentrations between 5 and 100 μg/mL and showed both an improvement in the cell proliferation of HDF cells and a decrease in the proliferation of cancerous cells when GREEN-TeNWs were compared with CHEM-TeNWs. An enhancement of healthy fibroblast proliferation was observed for the green synthesis of TeNWs compared with the CHEM-TeNWs, which suggests that these should be explored for a wide range of medical applications. Therefore, we propose that the present green synthetic approach offers important improvements in terms of safety, economy, efficiency, and biocompatibility for numerous biomedical applications, overcoming the main drawbacks of traditional Te nanowire chemical approaches.

## Acknowledgments

This work was supported by the Chemical Engineering Department at Northeastern University. Funding from MINECO (MAT2014-59772-C2-1-P and MAT2014-59772-C2-2-P) is acknowledged. We also thank the service from the MiNa Laboratory at Instituto de Micro y Nanotecnología funded by CM (S2013/ICE2822), MINECO (CSIC13-4E-1794), and the EU (FEDER, FSE). JMGM thanks MECD (PRX16/00383) and Fulbright Commission for his stay at Northeastern University.

JLCD acknowledges the financial support provided by the School of Engineering and Sciences of Tecnologico de Monterrey through the Research Group on Optics and Lasers. The authors thank Alfonso Nieto-Argüello for FT-IR spectroscopy and XRD measurements.

## Disclosure

Dr María Ujué González reports grants from MINECO, MINECO + EU, and the Government of Autonomous Region of Madrid, CM, during the conduct of the study. Dr Yves Huttel reports grants from MINECO during the conduct of the study. Dr José Miguel García-Martín reports grants from MINECO, MECD, and Fulbright Commission, during the conduct of the study. The authors report no other conflicts of interest in this work.

## References

1. North EJ, Halden RU. Plastics and environmental health: the road ahead. *Rev Environ Health*. 2013;28(1):1–8. doi:10.1515/reveh-2012-0030
2. Bijlsma N, Cohen MM. Environmental chemical assessment in clinical practice: unveiling the elephant in the room. *Int J Environ Res Public Health*. 2016;13(2):181. doi:10.3390/ijerph13020181
3. Lopez, JB, Jackson D, Gammie A, Badrick T, et al. Reducing the environmental impact of clinical laboratories. *Clin Biochem Rev*. 2017;38(1):3–11.
4. Wang L, Chen H, Shao L. The antimicrobial activity of nanoparticles: present situation and prospects for the future. *Int J Nanomedicine*. 2017;12:1227–1249. doi:10.2147/IJN.S121956
5. Hemeg H. Nanomaterials for alternative antibacterial therapy. *Int J Nanomedicine*. 2017;12:8211–8225. doi:10.2147/IJN.S132163

6. Graves, JL, Thomas M, Ewunkem J, et al. Antimicrobial nanomaterials: why evolution matters. *Nanomaterials(Basel)*. 2017;7(10):283.
7. Jain S, Hirst DG, O'Sullivan JM. Gold nanoparticles as novel agents for cancer therapy. *Br J Radiol*. 2012;85(1010):101–113. doi:10.1259/bjr/59448833
8. Cai W, Gao T, Hong H, Sun J. Applications of gold nanoparticles in cancer nanotechnology. *Nanotechnol Sci Appl*. 2008;1:17–32. doi:10.2147/NSA.S3788
9. Nune SK, Gunda P, Thallapally PK, Lin Y-Y, Laird Forrest M, Berkland CJ. Nanoparticles for biomedical imaging. *Expert Opin Drug Deliv*. 2009;6(11):1175–1194. doi:10.1517/17425240903229031
10. Estelrich J, Sánchez-Martín MJ, Busquets MA. Nanoparticles in magnetic resonance imaging: from simple to dual contrast agents. *Int J Nanomedicine*. 2015;10:1727–1741.
11. Choi HS, Frangioni JV. Nanoparticles for biomedical imaging: fundamentals of clinical translation. *Mol Imaging*. 2010;9(6):291–310.
12. Park K. Facing the truth about nanotechnology in drug delivery. *ACS Nano*. 2013;7(9):7442–7447. doi:10.1021/nn404501g
13. De Jong WH, Borm PJA. Drug delivery and nanoparticles: applicationsand Hazards. *Int J Nanomedicine*. 2008;3(2):133–149. doi:10.2147/IJN.S596
14. Wang, YF, Liu L, Xue X, Liang XJ. Nanoparticle-based drug delivery systems: what can they really do in vivo? *F1000Res*. 2017;6:681. doi:10.12688/f1000research.10493.2
15. Kögler, M, Ryabchikov YV, Uusitalo S, et al. Bare laser-synthesized Au-based nanoparticles as nondisturbing surface-enhanced raman scattering probes for bacteria identification. *J Biophotonics*. 2018: e201700225. doi:10.1002/jbio.201700225
16. Fernandez-Bravo A, Sivakumar P, Melikechi N, Mohamed AA. Femtosecond laser ablation synthesis of aryl functional group substituted gold nanoparticles. *J Nanosci Nanotechnol*. 2017;17(4):2852–2856. doi:10.1166/jnn.2017.13900
17. Bukhtiar A, Zou B. The preparation and optical properties of Ni(II) and Mn(II) doped in ZnTe nanobelt/nanorod by using chemical vapor deposition. *J Nanosci Nanotechnol*. 2018;18(7):4700–4713. doi:10.1166/jnn.2018.15283
18. Islam M, Achour A, Saeed K, Boujtita M, Javed S, Djouadi M. Metal/Carbon hybrid nanostructures produced from plasma-enhanced chemical vapor deposition over nafion-supported electrochemically deposited cobalt nanoparticles. *Materials*. 2018;11(5):687. doi:10.3390/ma11050687
19. Sudhakar A. History of cancer, ancient and modern treatment methods. *J Cancer Sci Ther*. 2009;1(2):1–4. PMC.
20. Arruebo, M, Vilaboa N, Sáez-Gutierrez B, et al. Assessment of the evolution of cancer treatment therapies. *Cancers*. 2011;3(3):3279–3330. doi:10.3390/cancers3033279
21. Aslan B, Ozpolat B, Sood AK, Lopez-Berestein G. Nanotechnology in cancer therapy. *J Drug Target*. 2013;21(10):904–913. doi:10.3109/1061186X.2013.837469.
22. Center for Disease Control and Prevention (CDC). Available from: https://www.cdc.gov/drugresistance/about.html. Assessed June 5, 2018.
23. Siegel RL, Miller KD, Jemal A. Cancer statistics, 2018. *CA Cancer J Clin*. 2018;68(1):7–30. doi:10.3322/caac.21442.
24. Ramirez LY, Huestis SE, Yap TY, Zyzanski S, Drotar D, Kodish E. Potential chemotherapy side effects: what do oncologists tell parents? *Pediatr Blood Cancer*. 2009;52(4):497–502. doi:10.1002/pbc.v52:4.
25. Baskar R, Lee KA, Yeo R, Yeoh K-W. Cancerand radiation therapy: current advances and future directions. *Int J Med Sci*. 2012;9(3): 193–199. doi:10.7150/ijms.3635.
26. Tohme S, Simmons RL, Tsung A. Surgery for cancer: a trigger for metastases. *Cancer Res*. 2017;77(7):1548–1552. doi:10.1158/0008-5472.CAN-16-1536
27. De Angelis C. Side effects related to systemic cancer treatment: are we changing the promethean experience with molecularly targeted therapies? *Current Oncol*. 2008;15(4):198–199.
28. Pearce, A, Haas M, Viney R, et al. Incidence and severity of self-reported chemotherapy side effects in routine care: a prospective cohort study. *PLoS One* 2017;12(10):e0184360. doi:10.1371/journal.pone.0184360
29. Shi J, Kantoff PW, Wooster R, Farokhzad OC. Cancer nanomedicine: progress, challenges and opportunities. *Nat Rev Cancer*. 2017;17:20–37. doi:10.1038/nrc.2016.108.
30. Gmeiner WH, Ghosh S. Nanotechnology for cancer treatment. *Nanatechnol Rev*. 2015;3(2):111–122.
31. Kulkarni N, Muddapur U. Biosynthesis of metal nanoparticles: a review. *J Nanotechnol*. 2014;2014:1–8. doi:10.1155/2014/510246
32. Ai J, Biazar E, Jafarpour M, et al. Nanotoxicology and Nanoparticle Safety in Biomedical Designs. *Int J Nanomedicine*. 2011;6:1117–1127. doi:10.2147/IJN.S25646
33. Shah M, Fawcett D, Sharma S, Tripathy S, Poinern G. Green synthesis of metallic nanoparticles via biological entities. *Materials*. 2015;8(11):7278–7308. doi:10.3390/ma8115377
34. Riehemann K, Schneider S, Luger T, Godin B, Ferrari M, Fuchs H. Nanomedicine-challenge and perspectives. *Angew Chem Int Ed*. 2009; 48(5):872–897. doi:10.1002/anie.v48:5
35. Hussain I, Singh NB, Singh A, Singh H, Singh SC. Green synthesis of nanoparticles and its potential application. *Biotechnol Lett*. 2016;38(4):545–560. doi:10.1007/s10529-015-2026-7
36. Cruz M, David GM, Webster TJ. Synthesis and characterization of biogenic selenium nanoparticles with antimicrobial properties made by *Staphylococcus Aureus*, Methicillin-Resistant *Staphylococcus Aureus* (MRSA), *Escherichia Coli*, and *Pseudomonas Aeruginosa*. *J Biomed Mater Res Part A*. 2018;106(5):1400–1412. doi:10.1002/jbm.a.36347
37. Larios-Rodriguez E, Rangel-Ayon C, Castillo SJ, Zavala G, Herrera-Urbina R. Bio-synthesis of gold nanoparticles by human epithelial cells, *in vivo*. *Nanotechnology*. 2011;22(35):355601. doi:10.1088/0957-4484/22/35/355601
38. El-Said WA, Cho H-Y, Yea C-H, Choi J-W. Synthesis of metal nanoparticles inside living human cells based on the intracellular formation process. *Adv Mater*. 2014;26(6):910–918. doi:10.1002/adma.v26.6
39. Molnár Z, Bódai V, Szakacs G, et al. Green synthesis of gold nanoparticles by thermophilic filamentous fungi. *Sci Rep*. 2018; 8(1):3943. doi:10.1038/s41598-018-22112-3
40. Makarov VV, Love AJ, Sinitsyna OV, et al. "Green" nanotechnologies: synthesis of metal nanoparticles using plants. *Acta Naturae*. 2014;6(1):35–44.
41. Singh P, Kim Y-J, Zhang D, Yang D-C. Biological synthesis of nanoparticles from plants and microorganisms. *Trends Biotechnol*. 2016;34(7):588–599. doi:10.1016/j.tibtech.2016.02.006
42. Dhand V, Soumya L, Bharadwaj S, Chakra S, Bhatt D, Sreedhar B. Green synthesis of silver nanoparticles using coffea Arabica seed extract and its antibacterial activity. *Mater Sci Eng C Mater Biol Appl*. 2016;58:36–43. doi:10.1016/j.msec.2015.08.018
43. Wu L, Cai X, Nelson K, et al. A green synthesis of carbon nanoparticles from honey and their use in real-time photoacoustic imaging. *Nano Res*. 2013;6(5):312–325. doi:10.1007/s12274-013-0308-8
44. Surendra TV, Roopan SM, Al-Dhabi NA, Arasu MV, Sarkar G, Suthindhiran K. Vegetable peel waste for the production of ZnO nanoparticles and its toxicological efficiency, antifungal, hemolytic, and antibacterial activities. *Nanoscale Res Lett*. 2016;11(1):546. doi:10.1186/s11671-016-1750-9
45. Gurunathan S, Han J, Park JH, Kim J-H. A green chemistry approach for synthesizing biocompatible gold nanoparticles. *Nanoscale Res Lett*. 2014;9(1):248. doi:10.1186/1556-276X-9-248
46. Mukherjee S, Sushma V, Patra S, et al. Green chemistry approach for the synthesis and stabilization of biocompatible gold nanoparticles and their potential applications in cancer therapy. *Nanotechnology*. 2012;23(45):455103. doi:10.1088/0957-4484/23/45/455103
47. Rehana D, Mahendiran D, Kumar RS, Rahiman AK. Evaluation of antioxidant and anticancer activity of copper oxide nanoparticles synthesized using medicinally important plant extracts. *Biomed Pharmacother*. 2017;89:1067–1077. doi:10.1016/j.biopha.2017.02.101
48. Kelkawi A, Abd H, Abbasi Kajani A, Bordbar A-K. Green synthesis of silver nanoparticles using mentha pulegium and investigation of their antibacterial, antifungal and anticancer activity. *IET Nanobiotechnol*. 2017;11(4):370–376. doi:10.1049/iet-nbt.2016.0103

49. Sudhasree S, Shakila Banu A, Brindha P, Kurian GA. Synthesis of nickel nanoparticles by chemical and green route and their comparison in respect to biological effect and toxicity. *Toxicol Environ Chem*. 2014;96(5):743–754. doi:10.1080/02772248.2014.923148
50. Liu T, Zhang G, Su X, Chen X, Wang D, Qin J. Tellurium nanotubes synthesized with microwave-assisted monosaccharide reduction method. *J Nanosci Nanotechnol*. 2007;7(7):2500–2505.
51. Tippayawat P, Phromviyo N, Boueroy P, Chompoosor A. Green synthesis of silver nanoparticles in aloe vera plant extract prepared by a hydrothermal method and their synergistic antibacterial activity. *PeerJ*. 2016;4:e2589. doi:10.7717/peerj.2589
52. Ramimoghadam D, Hussein MZB, Taufiq-Yap YH. Hydrothermal synthesis of zinc oxide nanoparticles using rice as soft biotemplate. *Chem Cent J*. 2013;7:136. doi:10.1186/1752-153X-7-136
53. Ji W, Qi W, Tang S, Peng H, Li S. Hydrothermal synthesis of ultrasmall Pt nanoparticles as highly active electrocatalysts for methanol oxidation. *Nanomaterials*. 2015;5(4):2203–2211. doi:10.3390/nano5042203
54. Hayashi H, Hakuta Y. Hydrothermal synthesis of metal oxide nanoparticles in supercritical water. *Materials*. 2010;3(7):3794–3817. doi:10.3390/ma3073794
55. Hong W, Wang J, Wang E. Facile synthesis of PdAgTe nanowires with superior electrocatalytic activity. *J Power Sources*. 2014;272:940–945. doi:10.1016/j.jpowsour.2014.09.029
56. Lu Q, Gao F, Komarneni S. A green chemical approach to the synthesis of tellurium nanowires. *Langmuir*. 2005;21(13):6002–6005. doi:10.1021/la050594p
57. Tsai HW, Yaghoubi A, Chan TC, et al. Electrochemical synthesis of ultrafast and gram-scale surfactant-free tellurium nanowires by gas-solid transformation and their applications as supercapacitor electrodes for p-doping of graphene transistors. *Nanoscale*. 2015;7(17):7535–7539. doi:10.1039/c5nr00876j
58. He Z, Yang Y, Liu JW, Yu SH. Emerging tellurium nanostructures: controllable synthesis and their applications. *Chem Soc Rev*. 2017;46(10):2732–2753. doi:10.1039/c7cs00013h
59. Ba LA, Döring M, Jamier V, Jacob C. Tellurium: an element with great biological potency and potential. *Org Biomol Chem*. 2010;8(19):4203–4216. doi:10.1039/c0Ob00086h.
60. Sredni B. Immunomodulating tellurium compounds as anti-cancer agents. *Semin Cancer Biol*. 2012;22(1):60–69. doi:10.1016/j.semcancer.2011.12.003
61. Abo Elsoud MM, Al-Hagar OEA, Abdelkhalek ES, Sidkey NM. Synthesis and investigations on tellurium myconanoparticles. *Biotechnol Rep*. 2018;18:e00247. doi:10.1016/j.btre.2018.e00247.
62. Chou T-M, Ke -Y-Y, Tsao Y-H, Li Y-C, Lin Z-HF. Abrication of Te and Te-Au nanowires-based carbon fiber fabrics for antibacterial applications. Ed. Jason K, Levy. *Int J Environ Res Public Health*. 2016;13(2):202. doi:10.3390/ijerph13020202
63. Silva RR, Mejia HAG, Ribeiro SJL, et al. Facile synthesis of tellurium nanowires and study of their third-order nonlinear optical properties. *J Braz Chem Soc*. 2017;28(1):58–67.
64. Liu Z, Shu L, Yang Y, et al. Shape-controlled synthesis and growth mechanism of one-dimensional nanostructures of trigonal tellurium. *New J Chem*. 2003;27:1748. doi:10.1039/b306782c.
65. Carotenuto G, Palomba M, De Nicola S, Ambrosone G, Coscia U. Structural and photoconductivity properties of tellurium/PMMA films. *Nanoscale Res Lett*. 2015;10:313. doi:10.1186/s11671-015-1007-z
66. El-Mallawany RA. Theoretical and experimental IR spectra of binary earth tellurite glasses. *Infrared Phys*. 1989;29:781–785. doi:10.1016/0020-0891(89)90125-5
67. Kizil R, Irudayaraj J, Seetharaman K. Characterization of irradiated starches by using FT-Raman and FTIR spectroscopy. *J Agric Food Chem*. 2002;50:3912–3918. doi:10.1021/jf011652p
68. Adenis C, Langer V, Lindqvist O. Reinvestigation of the structure of tellurium. *Acta Crystallogr C*. 1989;45:941–942. doi:10.1107/S0108270188014453
69. Velázquez JM, Gaikwad AV, Rout TK, Baier RE, Furlani ES, Banerjee S. Nanotexturation-induced extreme wettability of an elemental tellurium coating. *J Mater Chem*. 2012;22:3335–3339. doi:10.1039/C1JM14664E
70. Garcia R, Losilla NS, Martínez J, et al. Nanopatterning of carbonaceous structures by field-induced carbon dioxide splitting with a force microscope. *Appl Phys Lett*. 2010;96:143110. doi:10.1063/1.3374885
71. Nevshupa R, Martínez L, Álvarez L, et al. Influence of thermal ageing on surface degradation of ethylene-propylene-diene elastomer. *J Appl Polym Sci*. 2011;119:242–251. doi:10.1002/app.v119:1
72. Yang D, Wong WP. Small but mighty: nanoparticles probe cellular signaling pathways. *Dev Cell*. 2016;37(5):397–398. doi:10.1016/j.devcel.2016.05.021
73. Marano F, Hussain S, Rodrigues-Lima F, Baeza-Squiban A, Boland S. Nanoparticles: molecular targets and cell signalling. *Arch Toxicol*. 2011;85(7):733–741. doi:10.1007/s00204-010-0546-4
74. Sun H, Jia J, Jiang C, Zhai S. Gold nanoparticle-induced cell death and potential applications in nanomedicine. *Int J of Mol Sci*. 2018;19(3):E754.
75. Burattini S, Falcieri E. Analysis of cell death by electron microscopy. *Methods Mol Biol*. 2013;1004:77–89. doi:10.1007/978-1-62703-383-1_7
76. Taatjes DJ, Sobel BE, Budd RC. Morphological and cytochemical determination of cell death by apoptosis. *Histochem Cell Biol*. 2008;129(1):33–43. doi:10.1007/s00418-007-0356-9
77. Susan E. Apoptosis: A review of programmed cell death. *Toxicol Pathol*. 2007;35:495–516. doi:10.1080/01926230701320337

## Supplementary materials

X-ray diffraction peak list of identified samples:

1) Green-synthesized tellurium nanowires
2) Chemically synthesized tellurium nanowires

Peak list:

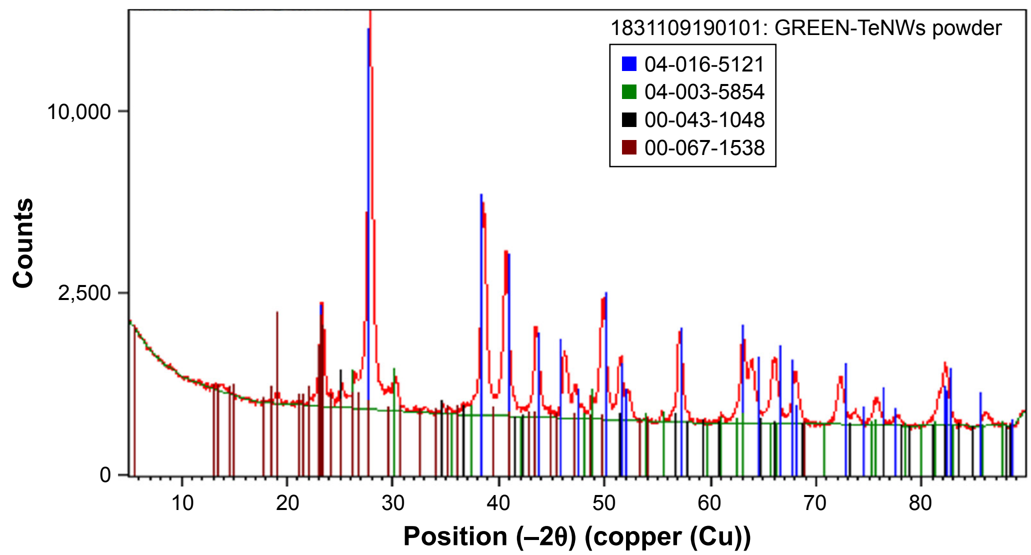


**Figure S1** XRD pattern for GREEN-TeNWs.

**Abbreviations:** GREEN-TeNWs, green-synthesized tellurium nanowires; XRD, X-ray powder diffraction.

**Table S1** Peak identification list for XRD pattern for GREEN-TeNWs

| Position (°2θ) | Height (cts) | FWHM left (°2θ) | d-spacing (Å) | Rel. Int. (%) | Tip width (°2θ) | Matched by |
|---|---|---|---|---|---|---|
| 13,1957 | 94,44 | 0,0768 | 6,70,966 | 0,59 | 0,0921 | 00-067-1538 |
| 13,8910 | 85,08 | 0,6140 | 6,37,530 | 0,53 | 0,7368 | |
| 19,1180 | 132,77 | 0,4605 | 4,64,242 | 0,83 | 0,5526 | 00-067-1538 |
| 21,0578 | 75,13 | 0,1919 | 4,21,896 | 0,47 | 0,2303 | 00-067-1538 |
| 23,2745 | 1901,95 | 0,3838 | 3,82,192 | 11,85 | 0,4605 | 04-016-5121, 00-067-1538 |
| 24,1109 | 164,10 | 0,1151 | 3,69,119 | 1,02 | 0,1382 | 00-067-1538 |
| 25,1056 | 299,79 | 0,3070 | 3,54,716 | 1,87 | 0,3684 | 00-043-1048, 00-067-1538 |
| 26,3655 | 453,76 | 0,2303 | 3,38,045 | 2,83 | 0,2763 | 04-003-5854, 00-067-1538 |
| 27,8158 | 16,047,72 | 0,3454 | 3,20,740 | 100,00 | 0,4145 | 04-016-5121, 00-067-1538 |
| 29,5937 | 288,81 | 0,1151 | 3,01864 | 1,80 | 0,1382 | 00-067-1538 |
| 30,1177 | 468,19 | 0,1535 | 2,96,730 | 2,92 | 0,1842 | 04-003-5854 |
| 30,4329 | 323,99 | 0,1535 | 2,93,728 | 2,02 | 0,1842 | |
| 32,0904 | 30,05 | 0,1535 | 2,78,925 | 0,19 | 0,1842 | |
| 32,9668 | 47,28 | 0,4605 | 2,71,708 | 0,29 | 0,5526 | |
| 34,7455 | 86,37 | 0,1535 | 2,58,195 | 0,54 | 0,1842 | 00-043-1048 |
| 35,3832 | 63,62 | 0,2303 | 2,53,687 | 0,40 | 0,2763 | 04-003-5854, 00-067-1538 |
| 36,5894 | 109,18 | 0,1151 | 2,45,596 | 0,68 | 0,1382 | 00-043-1048 |
| 38,5228 | 5267,40 | 0,3454 | 2,33,704 | 32,82 | 0,4145 | 04-016-5121 |
| 40,6315 | 3468,21 | 0,4221 | 2,22,048 | 21,61 | 0,5066 | 04-016-5121 |
| 43,5252 | 1440,62 | 0,3838 | 2,07933 | 8,98 | 0,4605 | 04-016-5121, 00-067-1538 |
| 44,8734 | 107,74 | 0,0768 | 2,01994 | 0,67 | 0,0921 | 00-043-1048, 00-067-1538 |
| 46,1746 | 863,30 | 0,3454 | 1,96,601 | 5,38 | 0,4145 | |

(*Continued*)

**Table S1** (*Continued*)

| Position (°2θ) | Height (cts) | FWHM left (°2θ) | d-spacing (Å) | Rel. Int. (%) | Tip width (°2θ) | Matched by |
|---|---|---|---|---|---|---|
| 47,3322 | 352,20 | 0,2686 | 1,92,059 | 2,19 | 0,3224 | 04-016-5121, 00-067-1538 |
| 47,9396 | 144,27 | 0,1151 | 1,89,767 | 0,90 | 0,1382 | 04-003-5854 |
| 48,6845 | 205,85 | 0,1535 | 1,87,036 | 1,28 | 0,1842 | 04-003-5854, 00-067-1538 |
| 49,7893 | 2084,93 | 0,4221 | 1,83,142 | 12,99 | 0,5066 | 00-067-1538 |
| 51,5206 | 817,40 | 0,3838 | 1,77,387 | 5,09 | 0,4605 | 04-016-5121, 00-043-1048 |
| 52,2020 | 312,70 | 0,1535 | 1,75,231 | 1,95 | 0,1842 | 04-016-5121 |
| 54,0039 | 39,28 | 0,3070 | 1,69,802 | 0,24 | 0,3684 | 04-003-5854, 00-067-1538 |
| 55,4375 | 104,24 | 0,1535 | 1,65,746 | 0,65 | 0,1842 | 04-003-5854 |
| 57,1566 | 1365,80 | 0,4221 | 1,61,163 | 8,51 | 0,5066 | 04-016-5121 |
| 58,3000 | 27,99 | 0,1919 | 1,58,272 | 0,17 | 0,2303 | |
| 61,0927 | 81,73 | 0,3838 | 1,51,689 | 0,51 | 0,4605 | 04-003-5854, 00-043-1048 |
| 63,0172 | 1213,72 | 0,2686 | 1,47,512 | 7,56 | 0,3224 | 04-016-5121, 04-003-5854 |
| 63,7614 | 778,02 | 0,2340 | 1,45,848 | 4,85 | 0,2808 | |
| 63,9862 | 769,47 | 0,1535 | 1,45,510 | 4,79 | 0,1842 | |
| 65,9294 | 779,38 | 0,2340 | 1,41,567 | 4,86 | 0,2808 | 04-003-5854, 00-043-1048 |
| 66,1437 | 825,67 | 0,2303 | 1,41,277 | 5,15 | 0,2763 | 04-003-5854, 00-043-1048 |
| 68,0895 | 579,45 | 0,3454 | 1,37,707 | 3,61 | 0,4145 | 04-016-5121 |
| 72,2240 | 506,74 | 0,1919 | 1,30,808 | 3,16 | 0,2303 | |
| 73,7367 | 119,08 | 0,4605 | 1,28,494 | 0,74 | 0,5526 | |
| 75,8096 | 262,89 | 0,6140 | 1,25,488 | 1,64 | 0,7368 | 04-003-5854 |
| 77,5390 | 115,96 | 0,1151 | 1,23,116 | 0,72 | 0,1382 | 04-016-5121 |
| 81,5887 | 282,16 | 0,1535 | 1,17,998 | 1,76 | 0,1842 | |
| 82,1625 | 782,00 | 0,1872 | 1,17,222 | 4,87 | 0,2246 | 04-016-5121, 00-043-1048 |
| 82,3791 | 688,99 | 0,1535 | 1,17,065 | 4,29 | 0,1842 | 04-016-5121, 00-043-1048 |
| 85,9082 | 104,27 | 0,5373 | 1,13,138 | 0,65 | 0,6447 | 04-016-5121, 04-003-5854 |

**Abbreviations:** GREEN-TeNWs, green-synthesized tellurium nanowires; FWHM, full width at half maximum; XRD, X-ray powder diffraction; Rel. Int., relative intensity.

**Table S2** List of identified patterns on XRD analysis of GREEN-TeNWs

| Reference code | Score | Compound name | Displacement (°2θ) | Scale factor | Chemical formula |
|---|---|---|---|---|---|
| 04-016-5121 | 44 | Tellurium | 0,000 | 0,840 | Te |
| 04-003-5854 | 36 | Tellurium oxide | 0,000 | 0,031 | $TeO_2$ |
| 00-043-1048 | 25 | Tellurium oxide | 0,000 | 0,028 | $TeO_3$ |
| 00-067-1538 | 30 | Poly(ethylene glycol) 7500 | 0,000 | 0,093 | $((CH_2)_2O)n$ |

**Abbreviations:** GREEN-TeNWs, green-synthesized tellurium nanowires; XRD, X-ray powder diffraction.

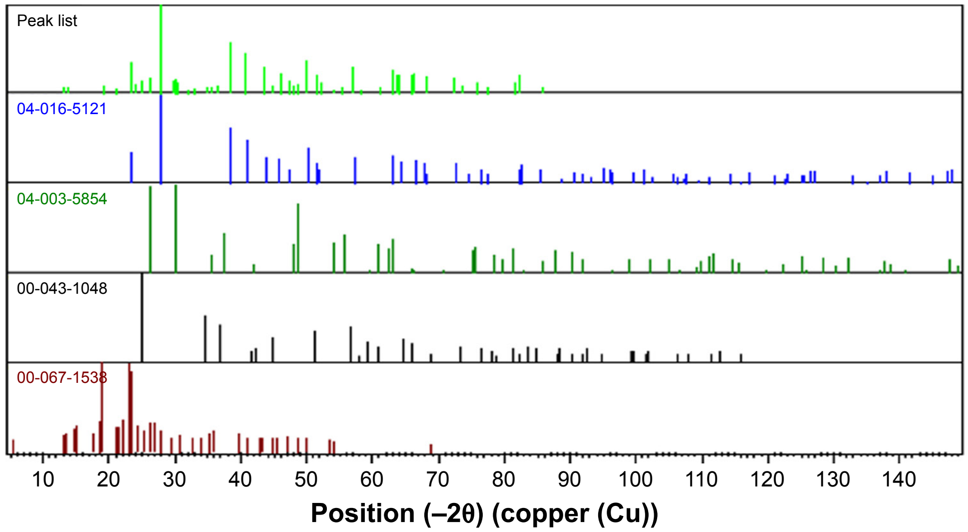


**Figure S2** XRD pattern for GREEN-TeNWs.
**Abbreviations:** GREEN-TeNWs, green-synthesized tellurium nanowires; XRD, X-ray powder diffraction.

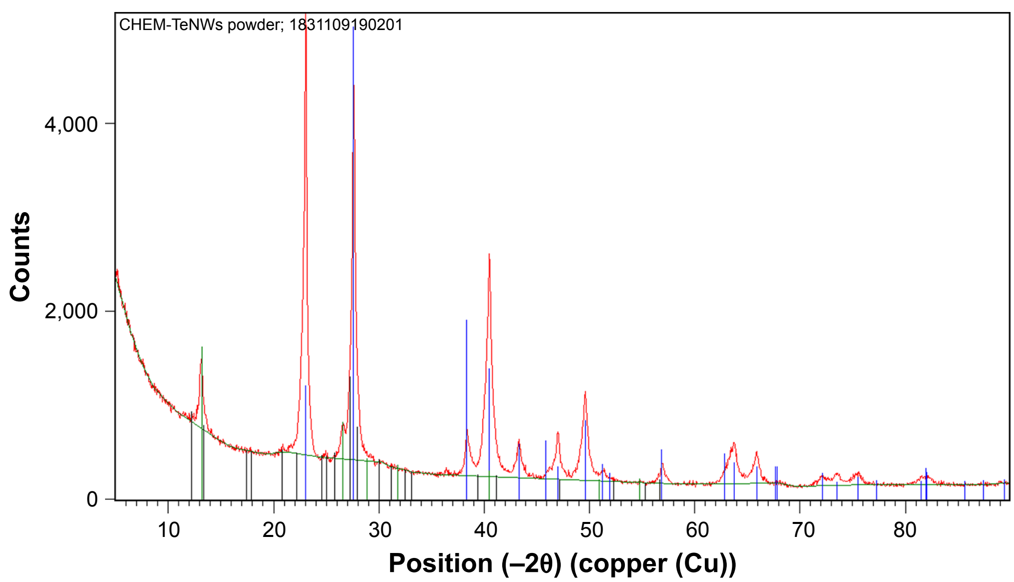


**Figure S3** XRD pattern for GREEN-TeNWs.
**Abbreviations:** GREEN-TeNWs, green-synthesized tellurium nanowires; XRD, X-ray powder diffraction.

**Table S3** Peak identification list for XRD pattern for CHEM-TeNWs

| Position (°2θ) | Height (cts) | FWHM (°2θ) | d-spacing (Å) | Rel. Int. (%) | Tip width (°2θ) | Matched by |
|---|---|---|---|---|---|---|
| 13,1969 | 741,73 | 0,2686 | 6,70,902 | 15,76 | 0,3224 | 00-032-1167; 00-054-1863 |
| 23,0429 | 4707,03 | 0,1535 | 3,85,981 | 100,00 | 0,1842 | 00-036-1452 |
| 26,6138 | 357,02 | 0,3454 | 3,34,947 | 7,58 | 0,4145 | 00-032-1167 |
| 27,5994 | 3979,25 | 0,1535 | 3,23,206 | 84,54 | 0,1842 | 00-036-1452 |
| 36,4139 | 50,56 | 0,2303 | 2,46,739 | 1,07 | 0,2763 | |
| 38,3353 | 482,31 | 0,1535 | 2,34,803 | 10,25 | 0,1842 | 00-036-1452 |
| 40,4878 | 2325,95 | 0,1919 | 2,22,803 | 49,41 | 0,2303 | 00-036-1452; 00-032-1167 |
| 43,3289 | 383,69 | 0,2303 | 2,08830 | 8,15 | 0,2763 | 00-036-1452 |
| 47,0262 | 505,58 | 0,2303 | 1,93,237 | 10,74 | 0,2763 | 00-036-1452; 00-054-1863 |
| 49,6237 | 941,80 | 0,1919 | 1,83,714 | 20,01 | 0,2303 | 00-036-1452 |
| 51,3913 | 116,05 | 0,3070 | 1,77,803 | 2,47 | 0,3684 | 00-036-1452 |
| 56,8808 | 221,45 | 0,2686 | 1,61,878 | 4,70 | 0,3224 | 00-036-1452; 00-054-1863 |
| 63,7370 | 438,99 | 0,2303 | 1,46,019 | 9,33 | 0,2763 | 00-036-1452 |
| 65,8686 | 324,54 | 0,2303 | 1,41,800 | 6,89 | 0,2763 | 00-036-1452 |
| 72,0718 | 98,14 | 0,3838 | 1,31,047 | 2,08 | 0,4605 | 00-036-1452 |
| 73,6438 | 114,88 | 0,5373 | 1,28,633 | 2,44 | 0,6447 | 00-036-1452 |
| 75,6068 | 136,85 | 0,3838 | 1,25,774 | 2,91 | 0,4605 | 00-036-1452 |
| 82,2074 | 76,41 | 1,6848 | 1,17,169 | 1,62 | 2,0218 | 00-036-1452 |

**Abbreviations:** CHEM-TeNWs, chemically synthesized tellurium nanowires; FWHM, full width at half maximum; XRD, X-ray powder diffraction; Rel. Int., relative intensity.

**Table S4** List of identified patterns on XRD analysis of CHEM-TeNWs

| Reference code | Score | Compound name | Displacement (°2θ) | Scale factor | Chemical formula |
|---|---|---|---|---|---|
| 00-036-1452 | 64 | Tellurium, syn | 0,000 | 0,890 | Te |
| 00-032-1167 | 43 | Sodium Tellurate Hydrate | 0,000 | 0,170 | $Na_2Te_4O_9$ 14.5 $H_2O$ |
| 00-054-1863 | 17 | 5,7-Dihydroxy-4H-4-chromenone | 0,000 | 0,281 | $C_9H_6O_4$ |

**Abbreviations:** CHEM-TeNWs, chemically synthesized tellurium nanowires; XRD, X-ray powder diffraction.

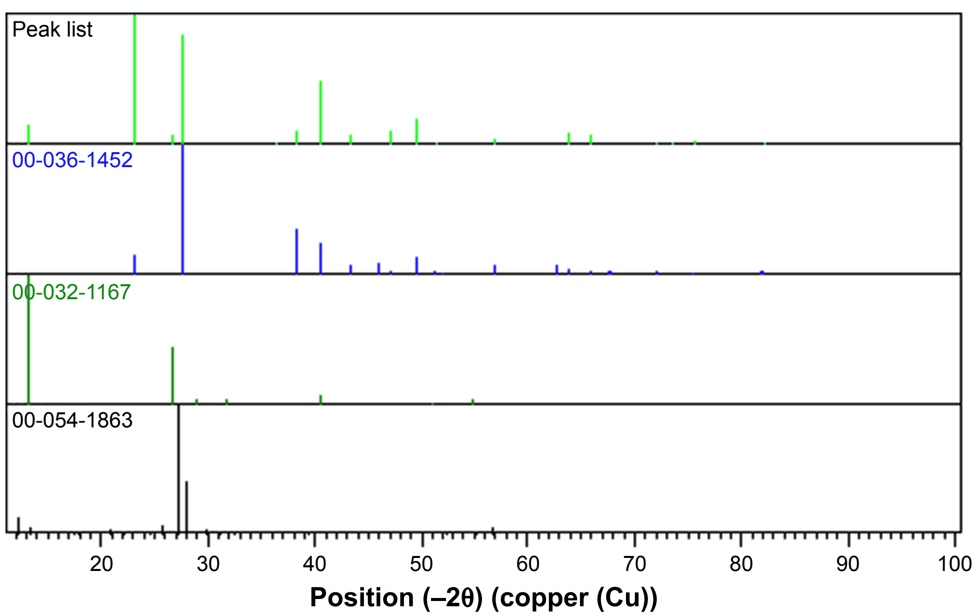


**Figure S4** XRD pattern for GREEN-TeNWs.
**Abbreviations:** GREEN-TeNWs, green-synthesized tellurium nanowires; XRD, X-ray powder diffraction.